PHYSICAL REVIEW D VOLUME 18, NUMBER 11 1 DECEMBER 1978

Differential cross sections for pion-proton bremsstrahlung at 269, 298, and 324 MeV

B. M. K. Nefkens, M. Arman,* H. C. Ballagh, Jr.,† P. F. Glodis, R. P. Haddock, K. C. Leung,‡ and D. E. A. Smith
Department of Physics, University of California, Los Angeles, California 90024

D. I. Sober
Department of Physics, University of California, Los Angeles, California 90024
and Department of Physics, The Catholic University of America, Washington, D.C. 20064 §

(Received 6 December 1977)

We present the results of new measurements of pion-proton bremsstrahlung ($\pi^+p \to \pi^+p\gamma$ and $\pi^-p \to \pi^-p\gamma$) at incident kinetic energies of 269 and 324 MeV, together with the final version of our earlier published results at 298 MeV. We have obtained differential cross sections over a wide range of photon angles, at photon energies between 15 and 150 MeV. The differential cross section in all 108 spectra decreases monotonically with increasing photon energy and its gross features agree with the external-emission-dominance calculation. Application of the model of Pascual and Tarrach to our data yields for the magnetic dipole moment of the $\Delta^{++}(1232)$ resonance the result $+4.7\mu_N < \mu_{\Delta^{++}} < 6.7\ \mu_N$, where $\mu_N = e\hbar/2m_pc$. This agrees with the SU(6) prediction of $+5.6\mu_N$.

I. INTRODUCTION

Interest in pion-proton bremsstrahlung ($\pi^+p \to \pi^+p\gamma$ and $\pi^-p \to \pi^-p\gamma$) in the region of the $\Delta(1232)$ resonance has centered on the following questions:

(a) How is the differential cross section affected by the final-state interaction due to the strong $\Delta(1232)$ resonance? Can one still use the soft-photon theorem, which is derived assuming nonresonant amplitudes?

(b) What is the range of photon energy for which the soft-photon approximation and the external-emission-dominance calculations are applicable?

(c) Can one determine the electromagnetic multipole moments of the $\Delta(1232)$, in particular its magnetic dipole moment?

(d) What can one learn about the off-mass-shell pion-nucleon interaction?

Prior to 1972, when the first publication[1] in the present series[1-5] appeared, the world's data for pion-proton bremsstrahlung ($\pi p\gamma$) consisted of 190 events.[6-10] We report here the final results of our measurements of $\pi p\gamma$ for π^+ and π^- incident beams at three energies in the region of the $\Delta(1232)$ resonance. We used an overconstrained detection system in which all three final-state particles were detected. We collected over 8000 $\pi p\gamma$ events and obtained the differential cross sections over a substantial region of the allowed kinematics, with enough statistics that at least some of the above questions can be answered.

In a bremsstrahlung process one can distinguish between two contributions: external radiation, in which the photon is emitted by an incident or outgoing charged particle, and internal radiation, in which the photon is coupled in some way to the internal structure of the interaction. The cross section for external bremsstrahlung accompanying a scattering process can be calculated from quantum electrodynamics. When the photon energy E_γ approaches zero the bremsstrahlung photon spectrum has a characteristic $1/E_\gamma$ dependence. More precisely, Low[11] has shown that in the limit $E_\gamma \to 0$, the first two terms in an expansion of the matrix element in the photon energy

$$M = \frac{a}{E_\gamma} + b \cdots \tag{1}$$

can be calculated exactly from the on-mass-shell elastic scattering amplitudes.

The use of the bremsstrahlung reaction to investigate the structure of the pion-nucleon interaction, or the properties of the Δ resonance, involves the detection of "internal" radiation and thus requires measurements at high photon energy, where the soft-photon theorem is invalid. To be most sensitive to internal-structure effects, the $\pi p\gamma$ cross section is measured in a geometry where the (calculable) external-bremsstrahlung contribution is minimal because of destructive interference between the contributing amplitudes. In our first experiment[1,2,4] (henceforth called I) at an incident energy of 298 MeV, we used ten photon counters which were clustered around an angle of 220° from the incident pion direction and 170° from the scattered pion direction. In this geometry there is maximal destructive interference in the $\pi^+p\gamma$ external radiation; this is discussed in Sec. V. Several calculations[12,13] had predicted that the $\pi^+p\gamma$ cross section for 300-MeV incident π^+ should show a pronounced bump in the photon spectrum near laboratory photon energy $E_\gamma \approx 60$ MeV, corresponding to an on-resonance final-state interaction in the process

$$\pi^+ p \to \Delta^{++} \to \Delta^{++}\gamma \to \pi^+ p\gamma \,, \tag{2}$$

with the magnitude of the bump providing a measurement of the magnetic dipole moment of the Δ^{++} resonance. Our first measurement[1] destroyed these expectations: the observed photon spectra in both $\pi^+ p\gamma$ and $\pi^- p\gamma$ decrease monotonically with increasing photon energy up to the highest measured photon energy of ≈ 120 MeV.

Our second experiment[3,5] (henceforth called II) was performed at the same incident energy of 298 MeV as I but with nine additional photon counters added at more forward angles where the external radiation contribution is larger. The results at forward photon angles show the same structureless falloff with photon energy as was seen at backward angles.

A number of model calculations have appeared since 1973[14-17] attempting to fit our results, but none has been very successful. A different approach, which bypasses most of the ambiuities inherent in hard-photon bremsstrahlung calculations, has recently been proposed by Pascual and Tarrach.[18] They interpret the absence of a bump or interference peak in $\pi p\gamma$ as evidence that reaction (2) is actually very small. Using the first two orders of the Low expansion, they can calculate the resonant contribution to the $\pi^+ p\gamma$ cross section in terms of the charges and magnetic moments of the π^+, p, and Δ^{++}. For a value of $\mu_{\Delta^{++}}$ around $+5.6\mu_N$, which happens to be the sign and magnitude predicted[19] by SU(6), the resonant contribution is very small, consistent with the absence of a large bump or interference in the photon spectra measured in our experiment. Furthermore, our $\pi^+ p\gamma$ data in the geometry of maximum destructive interference (see Sec. V) can be used to obtain surprisingly narrow limits for the magnitude of $\mu_{\Delta^{++}}$.

The most useful models for calculating the gross features of the $\pi p\gamma$ cross section have been those based on an extension of the Low theorem[11] to finite photon energy. Unfortunately, the extension procedure is neither rigorous nor unique. Some soft-photon-approximation (SPA) calculations[4,13] fit the results of experiments I and II well for the lowest photon energies, but become unreliable at higher photon energies where the second term of expansion (1) becomes important.

It was shown recently[20] that the first term of a suitable Low-type expansion of the bremsstrahlung cross section is highly successful in describing all photon spectra and angular distributions obtained in experiments I and II. This approximation, called external-emission dominance (EED), is particularly easy to calculate for all possible geometries: The bremsstrahlung cross section is simply equal to the elastic scattering cross section multiplied by a kinematic factor with no adjustable parameters. These and other theories will be discussed further in Sec. VI.

As much of the interest in our first $\pi p\gamma$ experiment is associated with the effects of the $\Delta(1232)$ resonance, we have supplemented the original measurements at $T_\pi = 298$ MeV with experiments at slightly higher and lower incident pion energy, thereby varying the relative contribution of the Δ in the πp amplitude. We report here the results of the new measurements at 324- and 269-MeV incident $\pi^\pm$ and compare them with results[1,4,5] at 298-MeV incident $\pi^\pm$, which have been revised to incorporate some improvements in the analysis.

II. APPARATUS AND EXPERIMENTAL METHOD

A plan view of our apparatus is shown in Fig. 1. Only the essential features of the equipment are discussed below; a more complete account of the setup has already been presented in I. The location of the photon, proton, and pion detectors is given in Table I in terms of d, α, and β. d is the distance from the front face of a photon counter to the center of the hydrogen target. α is the horizontal projection of the angle measured clockwise from the beam line. β is the angle of elevation measured upwards from the horizontal plane. The relation of α and β to the conventional polar and azimuth angles θ and ϕ is $\cos\theta = \cos\alpha\cos\beta$ and $\tan\phi = \tan\beta\csc\alpha$.

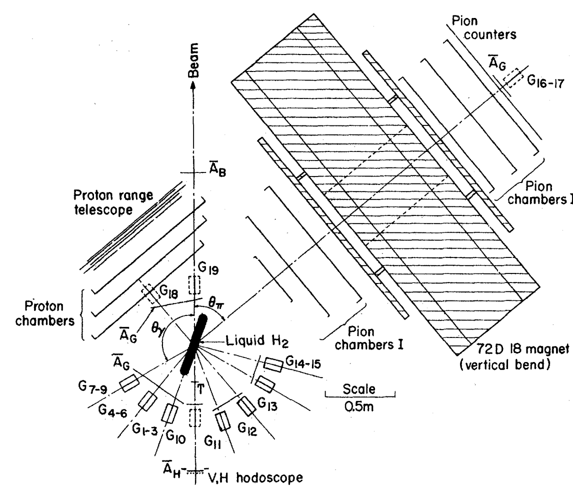

FIG. 1. Experimental apparatus. G_1 through G_{19} are lead-glass photon counters, of which G_1, G_4, G_7, and G_{11-14} lie in the horizontal plane. The pion and proton counters and chambers are described in the text. The position of each counter is given in Table I.

TABLE I. Position of particle detectors. α = horizontal projection of angle, measured clockwise from the beam line. β = angle of elevation, measured upwards from the horizontal plane. d = distance from center front face of photon counter to center of target.

	α (deg)	β (deg)	d (cm)
pion	50.5 ± 7.0	-10 to +24	73.8[a]
proton	323 ± 27	-26 to +26	92.1[b]
G_1	200.0	0	61.1
G_2	200.0	-18	56.0
G_3	200.0	-36	56.0
G_4	220.0	0	56.0
G_5	220.0	-18	56.0
G_6	220.0	-36	56.0
G_7	240.0	0	56.0
G_8	240.0	-18	56.0
G_9	240.0	-36	56.0
G_{10}	180.0	-36	56.0
G_{11}	160.0	0	63.0
G_{12}	140.0	0	63.0
G_{13}	120.0	0	63.0
G_{14}	103.0	0	63.0
G_{15}	103.0	-20	63.0
G_{17}	50.0	+4	300
G_{18}	320.0	-56	63.0
G_{19}	0	-59	63.0

[a] Distance to first pion spark chamber.
[b] Distance to first plane of counters.

A. Pion beam and target

The pions were produced in the external proton beam of the Lawrence Berkeley Laboratory 184-in. cyclotron. The parameters of the six pion beams are given in Table II. The π^+ beams had a 5.5-cm CH_2 degrader located at the intermediate focus to eliminate protons in the beam. The energy of each beam was determined from range measurements in copper. The range was converted to energy using the tables of Barkas and Berger[21] after correcting for multiple scattering, which at 300 MeV reduces the range by 2.8%.

The electron contamination of the beams was determined with a gas Cerenkov counter. The composition of the 324-MeV π^- beam was checked with the aid of a NaI counter and found to agree. The on-momentum muon contamination was extracted from the range curves while the fraction of off-momentum muons was calculated.

The liquid hydrogen target consisted of a flask with two flat, parallel walls of 0.13-mm-thick Mylar. It was surrounded by a cylindrical gas ballast of 0.25-mm-thick Mylar, and 21 layers of 6-μm aluminized Mylar located inside a cylindrical corrugated vacuum flask made of 0.8-mm-thick aluminum. The long axis of the target was inclined at an angle of $20.5 \pm 0.5°$ to the beam line so as to minimize the energy loss of the recoil proton in the hydrogen. The thickness of the flask was 6.5 cm, considerably more than previously reported[1-4] because of some unexpected bowing of the walls of the flask which was discovered after the completion of the experiment.

B. Counters and chambers

The incident pion direction was defined by the horizontal and vertical hodoscopes H and V, and by the timing counter T. H and V were surrounded by the anticounter $\overline{A}_H$ to eliminate the background produced by the beam halo.

The scattered pions were detected in a large magnetic spectrometer centered on an angle of 50.5° from the beamline. The main magnetic field was oriented horizontally so as to deflect the pions downward. The trajectory of each scattered pion was determined by a set of three wire spark chambers before the magnet and a set of three 1-m × 2-m chambers after the magnet. A set of four

TABLE II. Parameters of pion beams.

Particle	Kinetic energy[a] (MeV)	Laboratory momentum[b] (MeV/c)	Momentum spread (%)	Muon/pion ratio (%)	$e^{\pm}$/beam ratio (%)	Average rate (sec^{-1})	Production target
π^+	269 ± 4	384 ± 4	±3.3	5 ± 2	1.0 ± 0.5	1×10^6	48 cm CH_2
π^-	263 ± 5	378 ± 5	±4.5	5 ± 2	13 ± 2	2×10^5	25 cm Be
π^+	298 ± 3	414 ± 3	±2.6	4 ± 2.5	0.5 ± 0.5	8×10^5	48 cm CH_2
π^-	298 ± 3	414 ± 3	±2.6	4 ± 2.5	7.4 ± 1.0	1×10^5	15 cm Be
π^+	324 ± 4	442 ± 4	±1.7	3 ± 2	0.5 ± 0.5	2×10^6	33 cm CH_2
π^-	330 ± 4	448 ± 4	±3.3	3 ± 2	6 ± 2	1×10^5	17.8 cm Be + 5.5 cm CH_2

[a] At center of full liquid H_2 target.

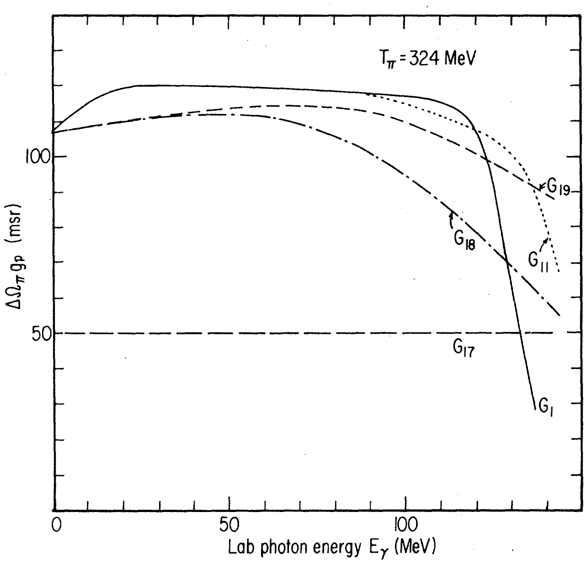

FIG. 2. Effective solid-angle acceptance for pions associated with five representative photon counters versus photon energy at $T_\pi = 324$ MeV. This effective solid angle takes into account the geometrical acceptance of the recoil protons. Furthermore, it is averaged over all interaction points in the target.

contiguous scintillation counters located behind the last chamber was used for triggering and for identifying pions by time-of-flight. The solid angle acceptance of the pion spectrometer was approximately 120 msr.

The proton detector consisted of three 1-m × 1-m wire spark chambers followed by a range telescope formed by six planes of scintillation counters plus copper absorbers. Only the first plane of counters was required in the event trigger; the counters were 6.4 mm thick and set to trigger on near minimum ionizing particles. The resolution of the range telescope was about ±10 MeV. The proton detector covered a solid angle of nearly 1 sr and did not limit the acceptance at most photon energies.

Photons were detected in 19 calibrated lead-glass Cerenkov counters G_1–G_{19}, each 10 cm × 10 cm in area and 15 cm (4.7 radiation lengths) thick. Charged particles entering the photon counters were vetoed by anticoincidence counters. The efficiency of the photon counters for on-axis photons, determined in a separate experiment,[22] was $(81 \pm 5)\%$ at $E_\gamma = 20$ MeV and $(92 \pm 2)\%$ at 50 MeV. Each counter (except G_{16} and G_{17}) subtended approximately ±5° horizontally and vertically from the center of the target. Photon counters G_{16} and G_{17} were located behind the pion spectrometer magnet, subtending only $\frac{1}{20}$ of the solid angle of the other photon counters. They required a substantial background subtraction owing to the interaction of pions in the surrounding shielding and, consequently, the results for G_{17} have very large error bars, and those for G_{16} will not be reported on here at all.

III. ANALYSIS

A. Kinematic reconstruction and event selection

The analysis procedure was essentially unchanged from that described in I. Proton and pion trajectories were reconstructed from the spark-chamber data and tested for consistency. The pion momentum was calculated from the angle of bend in the magnet. Each event was subjected to a two-constraint least-squares fit to the hypothesis $\pi p \to \pi p \gamma$ using the measured values of the direction and momentum of the incident and scattered pion and the directions of the photon and proton. The photon energy was calculated using parameters obtained in the least-squares fit.

Events with calculated photon energies below 15 MeV were rejected to avoid contamination of the bremsstrahlung sample by elastic scattering events with a random trigger in a photon counter. Cuts were made on photon time-of-flight (±6 nsec) and on the missing mass of the neutral particle to eliminate events due to $\pi p \to \pi p \pi^0$. In most cases, a small subtraction for photon counter randoms was also made, using the number of events per unit time outside the time-of-flight window as an estimate of the background. The final selection of events was performed by a cut on the χ^2-like variable (two degrees of freedom) which was minimized by the least-squares fit. Empty-target runs yielded a negligible number of accepted events, and it was not necessary to make an empty-target subtraction in this experiment.

The only substantial differences between the procedure for event selection described in I and that applied to the new experimental data are

(1) The final χ^2 cut, which was at 15 for most photon counters, was increased to 25 for counters G_{18} and G_{19} at the 269- and 298-MeV incident pion energies.

(2) The acceptance window on photon time of flight was varied slightly among the counters.

The photon energy resolution varied among the counters and was determined by analyzing $\pi p \to \pi p$ elastic scattering events as $\pi p \to \pi p \gamma$ events and calculating the fitted "photon" energy. Full width at half maximum was approximately 7 MeV for counters G_1–G_{12}, 12 MeV for G_{13}–G_{15}, 14 MeV for G_{18} and G_{19}, and 25 MeV for G_{17}. The poor resolution of G_{17} is responsible for the large error in the cross section for this counter in the lowest E_γ bin.

B. Cross-section calculation

The differential cross section in the laboratory system for $\pi^{\pm}p \to \pi^{\pm}p\gamma$ was calculated for each photon counter i and each interval of photon energy as

$$d\sigma_i(E_\gamma) \equiv \frac{d^5\sigma}{d\Omega_\pi d\Omega_\gamma dE_\gamma} = \frac{Y}{BT\Delta E_\gamma(\Delta\Omega_\pi g_p)_i(\Delta\Omega_\gamma\epsilon_\gamma)_i\epsilon_{sc}\epsilon_c\epsilon_{\text{surv}}} .$$

Y = number of events with photon energy between $E_\gamma - \frac{1}{2}\Delta E_\gamma$ and $E_\gamma + \frac{1}{2}\Delta E_\gamma$, corrected for small random time-of-flight background.

B = number of incident pions, obtained from the number of incident-beam particles corrected for electron and muon contamination, beam attenuation in the target, and loss of good events because of randoms in anti-counters and multiple incident-beam particles.

T = number of protons per unit area transverse to the beam in the hydrogen target. Using the revised thickness described in Sec. IIA, $T = (7.87 \pm 0.40) \times 10^{23}$ cm^{-2}.

ΔE_γ = width of photon energy interval (20 MeV in the present analysis, except for the lowest bin which is 15 MeV wide.)

$(\Delta\Omega_\pi g_p)$ = effective solid-angle acceptance for pions associated with each photon counter. It is the product of the solid-angle acceptance for pions and the geometric-acceptance factor for the recoil proton averaged over all interaction points in the target and calculated by Monte Carlo simulation of events.

$(\Delta\Omega_\gamma\epsilon_\gamma)_i$ = average solid angle times efficiency of photon counter i. The details of the efficiency calculation may be found in Ref. 22.

ϵ_{sc} = spark-chamber efficiency, which varied between 73% and 88% for the various data sets.

ϵ_c = efficiency of scintillation counters = $(98 \pm 2)\%$.

ϵ_{surv} = survival probability of outgoing particles as described in I. The losses were due to interactions of outgoing particles (12% to 18%) and to pion decay, which ranged from approximately 10% at $E_\gamma = 45$ MeV to 20% at $E_\gamma = 100$ MeV.

Tables of the numbers of accepted events and of the factors and corrections used in the cross-section calculation may be obtained from the authors.

IV. RESULTS

A. $\pi^{\pm}p \to \pi^{\pm}p\gamma$ cross sections

The laboratory differential cross section $d^5\sigma/d\Omega_\pi d\Omega_\gamma dE_\gamma$ for the various photon counters and for the various intervals of photon energy for the three incident beam energies for π^+ and π^- are given in Table III. There are two sets of results at 298 MeV for the photon counters $G_{1\text{-}10}$, previously published as Exp. I[4] and Exp. II[5] and presented here

TABLE III. $\pi p \to \pi p\gamma$ laboratory differential cross section $d^5\sigma/d\Omega_\pi d\Omega_\gamma dE_\gamma$ (in nb/sr^2 MeV) obtained for individual photon counters and for different intervals of photon energy. The last row gives the average over the 10 photon counters $G_{1\text{-}10}$ weighted by solid angle. The blank entries indicate that the acceptance is small.

Photon counter G	E_γ (MeV) 15–30	30–50	50–70	70–90	90–110	110–130	130–150
				269 MeV π^+			
1	1.0 ± 0.5	0.6 ± 0.4	0.9 ± 0.4	0.5 ± 0.3	0.2 ± 0.2		
2	0.9 ± 0.5	1.1 ± 0.4	1.2 ± 0.5	0.3 ± 0.2	0.2 ± 0.2		
3	3.1 ± 1.0	0.7 ± 0.3	1.1 ± 0.5	1.0 ± 0.4	0.6 ± 0.3	0.2 ± 0.2	
4	1.5 ± 0.9	1.2 ± 0.5	1.1 ± 0.4	0.3 ± 0.2	0.0 ± 0.2		
5	4.1 ± 1.2	1.4 ± 0.6	0.9 ± 0.5	0.3 ± 0.2	0.6 ± 0.3		
6	3.2 ± 1.0	0.9 ± 0.4	0.2 ± 0.2	1.1 ± 0.5	0.2 ± 0.2	0.7 ± 0.5	
7	1.6 ± 0.9	2.2 ± 0.7	1.9 ± 0.7	0.5 ± 0.3	0.3 ± 0.3		
8	2.8 ± 1.0	2.6 ± 0.8	2.2 ± 0.8	0.0 ± 0.3	0.0 ± 0.3		
9	3.1 ± 1.0	2.8 ± 0.9	1.4 ± 0.6	1.6 ± 0.7	0.0 ± 0.3		
10	3.6 ± 1.0	2.8 ± 0.8	1.6 ± 0.5	2.1 ± 0.7	0.8 ± 0.4	1.2 ± 0.5	
11	6.2 ± 1.5	3.6 ± 0.9	1.5 ± 0.6	0.8 ± 0.4	0.2 ± 0.2	0.0 ± 0.3	
12	16.5 ± 2.9	7.7 ± 1.5	4.2 ± 1.0	3.8 ± 0.9	0.6 ± 0.4	0 ± 0.2	
13	30.6 ± 4.8	14.4 ± 2.4	6.8 ± 1.4	6.1 ± 1.2	2.1 ± 0.7	0.7 ± 0.4	0 ± 0.2
14	51.6 ± 7.3	24.5 ± 3.5	16.7 ± 2.4	8.7 ± 1.5	4.0 ± 1.0	2.5 ± 0.8	0.7 ± 0.5
15	54.0 ± 7.6	25.2 ± 3.6	14.8 ± 2.2	9.5 ± 1.6	5.6 ± 1.2	2.9 ± 0.9	2.6 ± 0.9
17	410 ± 195	45 ± 42	95 ± 47	72 ± 28	52 ± 24	31 ± 18	0 ± 11
18	36.8 ± 6.1	27.8 ± 5.0	24.5 ± 5.4	19.4 ± 5.4	17.9 ± 5.8	13.7 ± 5.4	1.5 ± 1.5
19	72.4 ± 10.3	52.0 ± 7.6	38.1 ± 6.4	35.6 ± 7.1	19.1 ± 4.6	9.0 ± 2.8	5.0 ± 2.1
1–10	2.53 ± 0.41	1.65 ± 0.27	1.25 ± 0.21	0.79 ± 0.15	0.28 ± 0.08		

TABLE III. (*continued*)

Photon counter G	E_γ (MeV) 15–30	30–50	50–70	70–90	90–110	110–130	130–150
				263 MeV π^-			
1	1.1 ± 1.1	1.5 ± 1.1	0.7 ± 0.7	1.5 ± 1.0	0 ± 0.8		
2	2.8 ± 1.6	3.9 ± 1.6	1.3 ± 0.9	1.3 ± 0.9	0.7 ± 0.7		
3	5.8 ± 2.5	2.7 ± 1.4	0.7 ± 0.7	0.7 ± 0.7	0.7 ± 0.7		
4	6.0 ± 2.5	4.9 ± 1.9	0.7 ± 0.7	0 ± 0.7	0 ± 0.8		
5	6.8 ± 2.7	1.4 ± 1.0	2.3 ± 1.3	1.4 ± 1.0	0 ± 0.8	2.8 ± 2.8	
6	4.0 ± 2.1	4.5 ± 1.9	0.7 ± 0.7	0.8 ± 0.8	0.7 ± 0.7		
7	4.3 ± 2.7	4.9 ± 2.1	1.9 ± 1.4	3.8 ± 1.9	1.2 ± 1.2		
8	4.2 ± 2.1	4.1 ± 1.9	4.8 ± 2.2	1.0 ± 1.0			
9	7.3 ± 2.9	4.8 ± 2.0	1.8 ± 1.3	1.9 ± 1.4	1.0 ± 1.0		
10	2.7 ± 1.6	1.9 ± 1.1	2.6 ± 1.3	0.7 ± 0.7	0.6 ± 0.6	0 ± 0.8	
11	1.1 ± 2.0	2.3 ± 1.4	0.8 ± 0.8	0.8 ± 0.8			
12	5.7 ± 2.6	2.3 ± 1.4	1.6 ± 1.1	3.2 ± 1.6			
13	4.8 ± 2.5	1.6 ± 1.6	1.6 ± 1.6	3.3 ± 1.6			
14	6.0 ± 2.8	1.6 ± 1.2	6.5 ± 2.4	3.3 ± 1.7	0.9 ± 0.9	0.9 ± 0.9	
15	6.2 ± 2.9	7.5 ± 2.6	5.0 ± 2.1	3.3 ± 1.7	1.7 ± 1.2	0.9 ± 0.9	1.4 ± 1.4
17	63 ± 142	0 ± 42	78 ± 56	77 ± 55	0 ± 39	39 ± 40	0 ± 42
18	9.5 ± 4.2	7.7 ± 3.1	7.0 ± 3.4	8.4 ± 4.6	3.0 ± 3.1	17.1 ± 9.8	
19	32.6 ± 8.2	14.7 ± 4.2	17.8 ± 5.1	4.2 ± 2.5	1.7 ± 1.7	6.5 ± 3.9	7.8 ± 4.7
1–10	4.56 ± 0.88	3.48 ± 0.65	1.77 ± 0.42	1.28 ± 0.35	0.50 ± 0.21		
				298 MeV π^+ – Exp. I.			
1	1.08 ± 0.38	0.69 ± 0.20	0.69 ± 0.20	0.74 ± 0.20	0.21 ± 0.13	0.16 ± 0.12	
2	0.89 ± 0.34	0.58 ± 0.18	0.72 ± 0.20	0.41 ± 0.14	0.37 ± 0.13	0.25 ± 0.12	
3	1.73 ± 0.48	1.29 ± 0.28	0.73 ± 0.19	1.00 ± 0.23	0.85 ± 0.21	0.28 ± 0.13	
4	0.53 ± 0.25	0.81 ± 0.21	0.47 ± 0.15	0.37 ± 0.13	0.48 ± 0.15		
5	0.72 ± 0.31	0.87 ± 0.22	0.47 ± 0.17	0.67 ± 0.19	0.33 ± 0.14		
6	1.47 ± 0.36	0.77 ± 0.21	0.71 ± 0.19	0.64 ± 0.18	0.57 ± 0.17	0.57 ± 0.19	
7	1.88 ± 0.46	0.83 ± 0.22	0.95 ± 0.24	0.64 ± 0.19	0.62 ± 0.19		
8	1.68 ± 0.46	0.82 ± 0.22	1.41 ± 0.30	0.66 ± 0.20	0.57 ± 0.18		
9	2.66 ± 0.62	1.36 ± 0.32	1.78 ± 0.35	1.57 ± 0.33	0.89 ± 0.23	0.68 ± 0.23	
10	2.95 ± 0.57	1.75 ± 0.36	0.91 ± 0.23	0.98 ± 0.23	0.38 ± 0.14	0.1 ± 0.1	
1–10	1.57 ± 0.21	0.98 ± 0.12	0.89 ± 0.10	0.77 ± 0.08	0.55 ± 0.07	0.3 ± 0.1	
				298 MeV π^- – Exp. I.			
1	3.5 ± 2.5	3.9 ± 2.3	1.3 ± 1.3	1.3 ± 1.3	2.6 ± 1.9	0 ± 2.1	
2	3.1 ± 2.2	5.4 ± 2.5	2.2 ± 1.6	2.2 ± 1.6	1.1 ± 1.1	0 ± 1.4	
3	3.3 ± 2.3	5.6 ± 2.6	0 ± 1.1	2.3 ± 1.7	0 ± 1.2	0 ± 1.4	
4	6.5 ± 3.3	4.5 ± 2.3	2.3 ± 1.7	2.3 ± 1.6	0 ± 1.2		
5	3.2 ± 2.3	2.3 ± 1.6	1.2 ± 1.2	1.2 ± 1.2	2.4 ± 1.7		
6	1.6 ± 1.6	1.1 ± 1.1	2.3 ± 1.7	1.2 ± 1.2	0 ± 1.2	0 ± 1.6	
7	4.9 ± 2.9	1.2 ± 1.2	3.9 ± 2.3	1.3 ± 1.3	0 ± 1.4		
8	5.0 ± 2.9	2.4 ± 1.7	1.3 ± 1.3	4.1 ± 2.4	2.8 ± 2.0		
9	6.6 ± 3.4	9.6 ± 3.6	3.9 ± 2.3	1.3 ± 1.3	2.7 ± 1.9	0 ± 1.9	
10	6.5 ± 3.3	3.5 ± 2.0	3.4 ± 2.0	4.6 ± 2.3	0 ± 1.2	0 ± 1.3	
1–10	4.4 ± 1.0	3.9 ± 0.8	2.1 ± 0.6	2.2 ± 0.6	1.1 ± 0.4		

TABLE III. (*continued*)

Photon counter G	E_γ (MeV) 15–30	30–50	50–70	70–90	90–110	110–130	130–150
				298 MeV π^+ – Exp. II.			
1	0.5 ± 0.5	0.7 ± 0.4	0.5 ± 0.3	0.7 ± 0.4	0.4 ± 0.3	0 ± 0.3	
2	1.3 ± 0.5	0.7 ± 0.3	0.6 ± 0.3	0.6 ± 0.3	0.5 ± 0.3	0.4 ± 0.3	
3	3.6 ± 1.0	1.1 ± 0.4	1.2 ± 0.4	1.1 ± 0.4	0.5 ± 0.3	0.4 ± 0.3	
4	1.1 ± 0.5	0.9 ± 0.4	0.3 ± 0.2	0.2 ± 0.2	0.2 ± 0.2		
5	1.1 ± 0.7	0.6 ± 0.4	0.6 ± 0.3	0.6 ± 0.3	0 ± 0.2		
6	1.6 ± 0.6	1.1 ± 0.4	1.0 ± 0.4	0.7 ± 0.4	0.5 ± 0.3	0.9 ± 0.4	
7	1.8 ± 0.7	1.5 ± 0.5	1.4 ± 0.5	0.7 ± 0.4	0.4 ± 0.3		
8	2.0 ± 0.8	1.1 ± 0.5	1.4 ± 0.5	1.3 ± 0.5	0.8 ± 0.4		
9	2.0 ± 0.8	1.6 ± 0.6	1.6 ± 0.5	0.9 ± 0.4	0.6 ± 0.3	1.3 ± 0.6	
10	2.6 ± 0.8	1.3 ± 0.5	1.5 ± 0.5	0.6 ± 0.3	0.8 ± 0.4	0.5 ± 0.3	
11	4.9 ± 1.3	3.0 ± 0.8	1.5 ± 0.6	1.0 ± 0.4	0.4 ± 0.3	0 ± 0.2	
12	11.5 ± 2.3	4.8 ± 1.1	3.1 ± 0.8	2.1 ± 0.7	0.2 ± 0.2	0 ± 0.2	
13	24.7 ± 3.8	16.1 ± 2.3	9.0 ± 1.5	7.9 ± 1.4	2.4 ± 0.7	1.1 ± 0.5	0 ± 0.3
14	43.2 ± 5.7	25.1 ± 3.3	13.5 ± 1.9	8.5 ± 1.4	7.3 ± 1.3	1.3 ± 0.6	1.1 ± 0.5
15	40.6 ± 5.5	21.5 ± 2.9	11.0 ± 1.7	8.9 ± 1.5	6.6 ± 1.3	3.3 ± 0.9	0.3 ± 0.3
17	97 ± 198	133 ± 78	44 ± 44	108 ± 65	108 ± 49	87 ± 44	44 ± 31
18	31.5 ± 4.8	23.1 ± 3.2	21.8 ± 3.2	15.6 ± 2.9	13.2 ± 3.0	12.2 ± 3.2	6.9 ± 2.5
19	65.9 ± 8.4	41.0 ± 4.9	31.0 ± 3.6	27.2 ± 3.6	19.3 ± 3.0	11.2 ± 2.3	9.2 ± 2.2
1–10	1.78 ± 0.28	1.03 ± 0.17	1.03 ± 0.15	0.74 ± 0.13	0.44 ± 0.09	0.44 ± 0.12	
				298 MeV π^- – Exp. II.			
1	6.5 ± 3.3	2.4 ± 1.7	1.2 ± 1.2	1.2 ± 1.2	0 ± 1.2	0 ± 1.9	
2	5.7 ± 2.9	2.0 ± 1.4	3.1 ± 1.8	2.1 ± 1.5	0 ± 1.1	0 ± 1.4	
3	4.5 ± 2.7	3.1 ± 1.8	3.1 ± 1.8	2.2 ± 1.5	1.1 ± 1.1	1.3 ± 1.3	
4	7.4 ± 3.4	8.2 ± 3.0	0 ± 1.1	3.2 ± 1.8	1.1 ± 1.1		
5	4.4 ± 2.6	3.1 ± 1.8	1.1 ± 1.1	2.2 ± 1.5	1.1 ± 1.1		
6	9.1 ± 3.8	6.1 ± 2.6	1.1 ± 1.1	3.3 ± 1.9	1.1 ± 1.1	2.9 ± 2.1	
7	4.6 ± 2.7	8.8 ± 3.3	3.6 ± 2.1	2.4 ± 1.7	1.3 ± 1.3		
8	6.1 ± 3.1	5.4 ± 2.5	1.2 ± 1.2	5.0 ± 2.5	1.3 ± 1.3		
9	6.1 ± 3.1	6.6 ± 2.8	4.7 ± 2.4	2.4 ± 1.7	1.3 ± 1.3	1.7 ± 1.7	
10	3.0 ± 2.1	1.1 ± 1.1	3.1 ± 1.8	2.1 ± 1.5	1.1 ± 1.1	0 ± 1.2	
11	1.8 ± 1.8	1.3 ± 1.3	0 ± 1.3	0 ± 1.3	0 ± 1.4	0 ± 1.6	
12	3.7 ± 2.6	3.9 ± 2.3	3.9 ± 2.3	0 ± 1.3	0 ± 1.4	0 ± 1.6	
13	5.9 ± 3.5	7.9 ± 3.3	7.9 ± 3.3	1.3 ± 1.3	0 ± 1.4	0 ± 1.5	0 ± 2.3
14	6.1 ± 3.6	5.4 ± 2.8	1.3 ± 1.3	4.2 ± 2.3	2.9 ± 2.0	1.5 ± 1.5	0 ± 1.8
15	14.0 ± 5.5	5.4 ± 2.8	1.4 ± 1.4	2.7 ± 1.9	1.4 ± 1.4	3.1 ± 2.2	0 ± 1.8
17	93 ± 94	0 ± 64	0 ± 63	62 ± 63	0 ± 63	0 ± 63	0 ± 65
18	16.5 ± 6.1	5.8 ± 2.9	11.4 ± 4.5	14.0 ± 5.6	12.7 ± 6.0	10.3 ± 6.2	4.7 ± 4.8
19	26.3 ± 7.8	15.4 ± 4.9	9.9 ± 3.8	4.6 ± 2.7	5.2 ± 3.1	4.1 ± 2.9	8.2 ± 4.8
1–10	5.7 ± 1.1	4.7 ± 0.9	2.2 ± 0.5	2.6 ± 0.6	0.94 ± 0.34	0.61 ± 0.31	
				324 MeV π^+			
1	2.4 ± 1.3	0 ± 0.5	0.6 ± 0.5	0.4 ± 0.4	0 ± 0.4	0 ± 0.4	
2	0.4 ± 0.7	0.8 ± 0.5	1.1 ± 0.6	0.6 ± 0.4	0 ± 0.3	0 ± 0.3	
3	2.4 ± 1.0	1.4 ± 0.7	0.6 ± 0.4	1.2 ± 0.6	0 ± 0.3	0 ± 0.3	
4	0 ± 1.1	1.4 ± 0.7	0 ± 0.3	0.9 ± 0.5	0 ± 0.3	0 ± 0.4	
5	0.9 ± 0.8	0.6 ± 0.4	0.1 ± 0.3	0.3 ± 0.3	0.6 ± 0.4	0 ± 0.4	
6	0.8 ± 0.6	0.3 ± 0.3	0.6 ± 0.4	0.3 ± 0.3	0.3 ± 0.3	0 ± 0.3	
7	0.4 ± 0.9	0.6 ± 0.4	0.5 ± 0.4	1.0 ± 0.6	0.3 ± 0.3	0 ± 0.5	

TABLE III. (*continued*)

Photon counter G	15–30	30–50	50–70	70–90	90–110	110–130	130–150
				E_γ (MeV)			
				324 MeV π^+			
8	0.7 ± 0.7	1.5 ± 0.8	0.6 ± 0.4	0.3 ± 0.3	0 ± 0.3	0 ± 0.4	
9	0.5 ± 0.9	1.1 ± 0.6	1.8 ± 0.8	2.4 ± 0.9	1.4 ± 0.8	0.7 ± 0.5	
10	2.0 ± 0.9	2.6 ± 1.0	0.9 ± 0.5	0.3 ± 0.3	0.3 ± 0.3	0.3 ± 0.3	0 ± 0.3
11	3.4 ± 2.5	0.5 ± 1.2	0.5 ± 0.6	0 ± 0.4	0 ± 0.4	0 ± 0.4	0 ± 0.4
12	15.5 ± 3.8	2.6 ± 1.1	2.6 ± 1.0	1.1 ± 0.7	0 ± 0.4	0 ± 0.4	0 ± 0.4
13	25.8 ± 5.3	9.9 ± 2.4	6.7 ± 1.9	4.1 ± 1.4	1.2 ± 0.7	0.4 ± 0.4	0.5 ± 0.5
14	24.8 ± 5.8	15.6 ± 3.3	4.0 ± 1.3	2.3 ± 1.0	2.8 ± 1.1	1.2 ± 0.7	0.5 ± 0.5
15	43.6 ± 8.2	12.9 ± 3.0	10.2 ± 2.5	3.6 ± 1.3	4.2 ± 1.5	1.3 ± 0.8	0.9 ± 0.7
17	157 ± 68	58 ± 35	57 ± 34	19 ± 19	0 ± 17	0 ± 19	0 ± 16
18	20.3 ± 5.6	13.5 ± 3.0	5.5 ± 1.6	11.1 ± 2.7	8.6 ± 2.4	11.1 ± 3.0	4.4 ± 1.9
19	47.4 ± 9.2	30.2 ± 5.5	25.5 ± 4.7	23.3 ± 4.5	21.9 ± 4.3	13.3 ± 3.2	14.4 ± 3.5
1–10	1.05 ± 0.31	1.04 ± 0.22	0.66 ± 0.17	0.77 ± 0.18	0.30 ± 0.11	0.10 ± 0.06	
				330 MeV π^-			
1	4.9 ± 3.5	8.5 ± 4.0	0 ± 1.7	0 ± 1.8	1.9 ± 1.9	0 ± 2.1	
2	0 ± 2.1	1.5 ± 1.5	1.5 ± 1.5	0 ± 1.5	0 ± 1.6	0 ± 1.8	
3	2.1 ± 2.2	1.5 ± 1.6	2.9 ± 2.1	0 ± 1.6	0 ± 1.7	1.7 ± 1.7	
4	2.0 ± 2.1	0 ± 1.5	1.5 ± 1.5	1.6 ± 1.6	1.6 ± 1.6	0 ± 2.3	
5	0 ± 2.2	0 ± 1.5	0 ± 1.5	1.6 ± 1.6	1.6 ± 1.6	0 ± 2.0	
6	0 ± 2.2	2.9 ± 2.0	0 ± 1.5	0 ± 1.6	0 ± 1.6	0 ± 1.7	
7	6.6 ± 3.9	1.5 ± 1.5	1.5 ± 1.5	4.4 ± 2.6	4.7 ± 2.8	0 ± 2.3	
8	2.3 ± 2.3	6.1 ± 3.1	2.9 ± 2.1	5.1 ± 3.0	3.2 ± 2.3	2.1 ± 2.1	
9	8.7 ± 4.5	0 ± 1.4	0 ± 1.5	0 ± 1.5	0 ± 1.6	0 ± 1.8	
10	2.1 ± 2.1	4.6 ± 2.7	7.4 ± 3.4	1.6 ± 1.6	1.7 ± 1.7	0 ± 1.8	0 ± 1.6
11	2.7 ± 2.7	0 ± 1.9	1.8 ± 1.8	0 ± 1.9	0 ± 2.1	0 ± 2.3	0 ± 2.3
12	2.8 ± 2.8	0 ± 1.8	1.9 ± 1.9	1.9 ± 1.9	0 ± 2.1	0 ± 2.3	0 ± 2.1
13	2.8 ± 2.8	7.6 ± 3.9	0 ± 1.9	1.9 ± 2.0	0 ± 2.1	0 ± 2.2	0 ± 1.9
14	0 ± 3.0	3.9 ± 2.8	5.7 ± 3.4	0 ± 2.0	0 ± 2.1	0 ± 2.3	0 ± 1.9
15	15.4 ± 7.2	11.9 ± 5.1	0 ± 2.0	6.0 ± 3.5	0 ± 2.1	0 ± 2.3	0 ± 1.8
17	138 ± 140	0 ± 102	0 ± 100	0 ± 99	0 ± 90	0 ± 99	0 ± 86
18	24.3 ± 9.2	6.1 ± 3.6	2.0 ± 2.1	9.1 ± 4.7	2.5 ± 2.5	0 ± 3.1	7.7 ± 5.6
19	12.0 ± 6.2	6.1 ± 3.6	9.7 ± 4.5	8.2 ± 4.2	6.5 ± 3.9	2.5 ± 2.5	2.6 ± 2.6
1–10	2.9 ± 0.9	2.6 ± 0.7	1.8 ± 0.6	1.5 ± 0.5	1.5 ± 0.5	0.4 ± 0.3	

TABLE IV. Laboratory to center-of-mass conversion factors. $1/J$ is that factor by which to multiply the laboratory cross section (Table III) to convert it to the cross section in the c.m. system. $J = d\sigma\,(\text{lab})/d\sigma\,(\text{c.m.}) = d\Omega_\pi^* d\Omega_\gamma^* dE_\gamma^* / d\Omega_\pi d\Omega_\gamma dE_\gamma$, where the starred variables are evaluated in the c.m. system.

	T_π = 269 MeV				T_π = 324 MeV			
		$1/J$				$1/J$		
Photon counter	E_γ (c.m.)/E_γ (lab)	22.5 MeV	50 MeV	100 MeV	E_γ (c.m.)/E_γ (lab)	22.5 MeV	50 MeV	100 MeV
1-3	1.31	0.92	0.91	0.86	1.35	0.94	0.93	0.90
4-6	1.26	0.89	0.88	0.83	1.30	0.90	0.89	0.87
7-9	1.19	0.83	0.83	0.81	1.21	0.85	0.84	0.82
10, 11	1.30	0.90	0.89	0.84	1.34	0.92	0.92	0.89
12	1.27	0.90	0.88	0.83	1.31	0.91	0.90	0.87
13	1.19	0.83	0.82	0.78	1.22	0.85	0.84	0.82
14, 15	1.12	0.78	0.77	0.83	1.14	0.79	0.78	0.76
17	0.85	0.61	0.60	0.58	0.84	0.59	0.58	0.57
18, 19	0.92	0.65	0.64	0.63	0.91	0.64	0.64	0.64

with the final corrections. They will be compared with each other in the next section. The data in Table III supersede all previously published results.

Our choice of the laboratory system for quoting the results of the three-body final-state reaction is prompted by the fact that the geometric acceptance of the three detectors is nearly constant in the lab system. The Jacobian does not vary very much in our experiment so the gross features of the differential cross section in the lab are similar to those in the center-of-mass. The Jacobian factors to convert the lab cross section and the lab photon energy to the center-of-mass system are given in Table IV.

B. Comparison of experiment I and experiment II

Prior to this paper, we have published the results from two separate measurements of $\pi^{\pm}p\gamma$ at $T_\pi = 298$ MeV: Experiment I[4] included only photon counters G_1-G_{10}, while Exp. II[5] included all 19 counters. Thus, there are two separate determinations of the cross sections for counters G_1 through G_{10} at $T_\pi = 298$ MeV. The results of both experiments are listed in Table III and illustrated in Fig. 3. The agreement between the two sets of data is excellent. Note that the statistical errors for the π^+ data of Exp. II are larger than those of Exp. I.

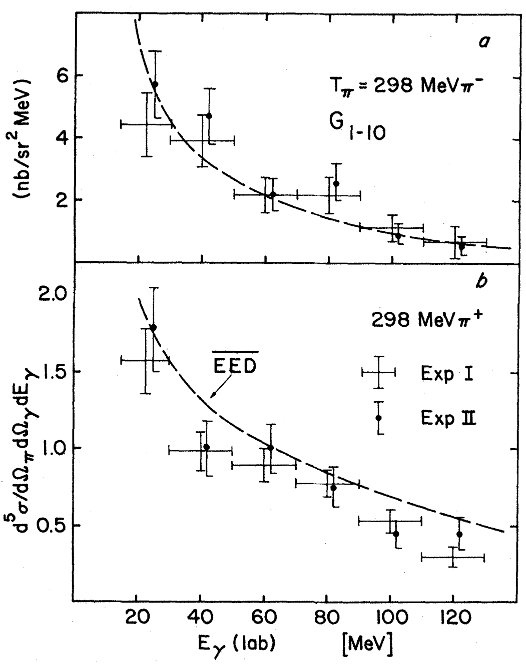

FIG. 3. $\pi^{\pm}p\gamma$ laboratory differential cross section averaged over the 10 "backward-angle" photon counters G_{1-10} at $T_\pi = 298$ MeV, revised results of Exps. I and II, with II displaced horizontally for clarity. The dashed curve is the $\overline{\mathrm{EED}}(\bar{s},\bar{t})$ calculation (Sec. VI A).

The data of Exp. I presented here have been reanalyzed since the publication of I, yielding similar results for the $\pi^+p\gamma$ cross section in spite of two changes. Between the publication of I and II, it was discovered that the supposedly flat walls of the hydrogen target flask exhibited substantial curvature under the small pressure of the hydrogen in the reservoir, increasing the effective thickness of the target by 28% from the originally quoted value. However, reanalysis of the data showed that in the production of intermediate good event tapes for $\pi^+p\gamma$ in Exp. I, approximately 21% of the good events were lost to excessively stringent cuts. The result of these changes, together with a slight improvement in the calculation of pion decay and some other small corrections, is that the reanalyzed Exp. I $\pi^+p\gamma$ cross sections are not substantially different from those published in Ref. 4 and are in excellent agreement with the cross section for G_1-G_{10} as measured in Exp. II. The new Exp. I $\pi^-p\gamma$ cross sections are nearly 28% smaller than those originally reported,[4] and the agreement with Exp. II is very good.

C. $\pi^{\pm}p$ elastic scattering results

We have measured the $\pi^{\pm}p\to\pi^{\pm}p$ differential cross section with our apparatus by taking some data with the photon counters removed from the coincidence logic. The horizontal acceptance of the spectrometer subtends a range of ±7° in the laboratory. Although the pion spectrometer is centered at 50.5° to the beam, the effective average scattering angle in our experiment is 52° (lab) because of the large vertical acceptance of the spectrometer. Our results for $d\sigma/d\Omega$ in the c.m. system are presented in Table V. For comparison, we have included the values reported by Bussey *et al.*,[23] extrapolated to our beam energy and scattering angle, except at 324 MeV where there are no accurate measurements available and the values listed are based on the Saclay phase shifts.[24]

Our elastic scattering results at $T_\pi = 263$, 298, 324 MeV are about 10% lower than the literature values[23,24]; the difference falls within the systematic errors of our experiment and the uncertainties of the extrapolation of the results in the literature. The π^+p measurement at $T_\pi = 269$ MeV is two standard deviations below the value of Bussey *et al.*,[23] a difference which is substantial but not unacceptable. The only serious discrepancy occurs for the π^-p measurement at $T_\pi = 300$ MeV, which is 38% lower than the phase-shift prediction. We note that the phase shifts in this energy region are dominated by a single old experiment at 310 MeV, which does not agree with

TABLE V. $\pi^+ p$ elastic cross sections. The cross sections are averaged over a range of angles corresponding to ± 0.14 in $\cos\theta_{c.m.}$ due to the large acceptance of our spectrometer. The central angle corresponds to $\theta_{lab} = 52°$.

Incident particle	Beam energy (MeV)	Beam momentum (MeV/c)	$\langle\cos\theta\rangle_{c.m.}$	This experiment (mb/sr)	Others (mb/sr)
π^+	269	384	0.35	5.3 ± 0.6	6.5[a]
π^+	298	414	0.36	4.7 ± 0.4	5.1[a]
π^+	324	442	0.37	3.7 ± 0.4	4.2[b]
π^-	263	378	0.35	0.77 ± 0.08	0.85[a]
π^-	298	414	0.36	0.72 ± 0.06	0.80[a]
π^+	330	448	0.37	0.68 ± 0.07	0.94[b]

[a] Extrapolated from Bussey *et al.* (Ref. 23).
[b] Estimated from Saclay phase shifts (Ref. 24).

the preliminary results of a recent experiment by V. A. Gordeev *et al.*[25] and does not appear to be consistent with the measurements of Bussey *et al.*

D. Discussion of errors

As discussed in the preceding section, our elastic-scattering cross-section measurements are approximately 10% lower than previously existing elastic scattering data. Although the latter are not fully internally consistent, and although the error in our elastic cross-section measurements is estimated at about 10%, the systematic discrepancy raises the possibility that all our cross sections, both elastic and $\pi p\gamma$, might be systematically 10% low. Such an error could be attributed to any of the normalization factors, such as effective target thickness, solid-angle acceptance, etc. While such an effect is annoying, we do not consider it to be a serious cause for concern, especially as the statistical errors in the $\pi p\gamma$ differential cross section are always considerably greater than 10%. We note that the comparisons of $\pi p\gamma$ data with the particular form of the EED theory which we label EED* (see Sec. V C)are independent of such a normalization error, since the EED* calculations are normalized to our measured elastic cross sections.

V. DISCUSSION OF EXPERIMENTAL RESULTS

A. Photon angular distribution

The measured differential cross sections given in Table III show a rapid variation of the cross section with photon angle. To help understand this and other phenomena, we shall make a comparison with EED calculations discussed below in Sec. VI. They give a fair representation of our data and provide a simple interpretation of some of the striking features observed.

Shown in Fig. 4 is the EED calculation of the differential cross section for 269-MeV incident π^+ and π^-, as a function of the horizontal angle α_γ for 22.5-MeV photons in a fictitious coplanar "point geometry" in which the pion is scattered at $\alpha_\pi = 50.5°$ and $\beta_\pi = 0°$, and the photon emerges in the horizontal plane. Curves for other incident energies and other E_γ are very similar and are not shown. The peak in the spectrum near $\alpha_\gamma = 22°$ can be identified with the forward bremsstrahlung cone of the incoming and outgoing pion; the peak near $\alpha_\gamma = 337°$ is due to the proton forward cone. The height of the peak is roughly proportional to the

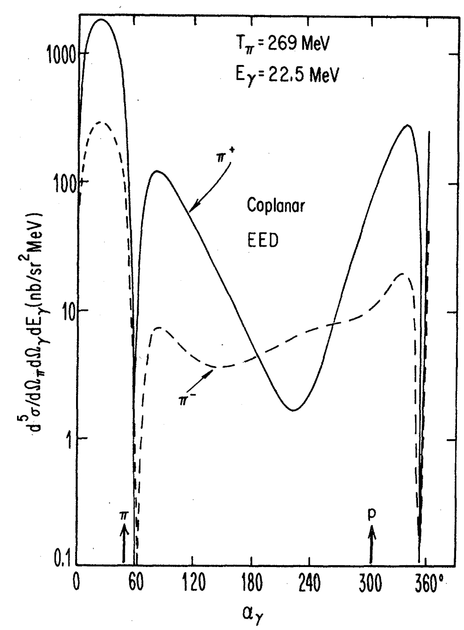

FIG. 4. Theoretical $\pi^+ p\gamma$ and $\pi^- p\gamma$ angular distributions. The laboratory differential cross section is given as a function of the horizontal photon angle α_γ for 22.5-MeV photons at $T_\pi = 269$ MeV, calculated using EED$(\bar{s}, \bar{t})$ for a coplanar point geometry. The vertical arrows marked π and p on the abscissa show the location of the pion and proton detector.

elastic cross section. Consequently, $d^5\sigma(\pi^+p\gamma)$ is larger than $d^5\sigma(\pi^-p\gamma)$ at these maxima. The big dip near $\alpha_\gamma = 220°$ in the $\pi^+p\gamma$ cross section is due to the destructive interference of the pion and proton backward bremsstrahlung amplitudes. In contrast, there is constructive interference of these amplitudes in $\pi^-p\gamma$, and there is no dip in the $\pi^-p\gamma$ cross section near $\alpha_\gamma = 220°$; note that $d^5\sigma(\pi^-p\gamma) > d^5\sigma(\pi^+p\gamma)$. The steep, deep dips near $\alpha_\gamma = 60°$ and 355° for both π^+ and π^- are characteristic of a coplanar geometry and disappear quickly when the geometry is slightly modified to a noncoplanar one. Fortunately, the big dip in the $\pi^+p\gamma$ cross section near $\alpha_\gamma = 220°$ is not strongly dependent on the geometry being coplanar and enables us to use large detectors. This dip region is therefore favored when searching for the magnetic dipole radiation from the $\Delta^{++}(1232)$ resonance and for "internal" radiation in general.

Figure 5 shows the experimental results for $T_\pi = 269$ MeV. The data for all photon counters with the same α_γ have been averaged. The curve is a coplanar EED* calculation, as described in Sec. C. The crosses represent the Monte Carlo averaged EED* calculation for the actual counter geometry. Note that counters G_{18} and G_{19} (at $\alpha_\gamma = 320°$ and 360°) are, respectively, 56° and 59° below the horizontal plane, so that large deviations from the "coplanar" curve are fully expected (note the crosses).

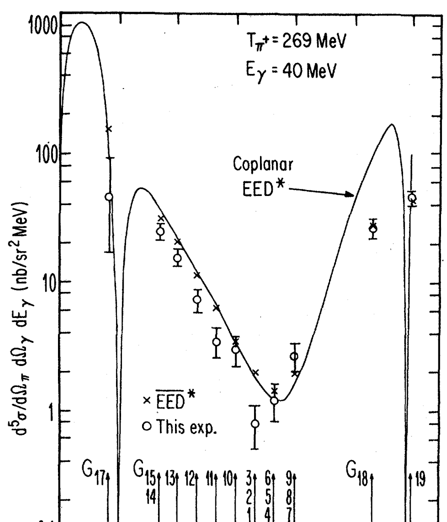

FIG. 5. Laboratory angular distribution of the $\pi^+p\gamma$ differential cross section of 40-MeV photons at $T_\pi = 269$ MeV. The open circles are the experimental data, averaged over all photon counters with the same α_γ. The crosses mark the $\overline{\text{EED}}$* prediction, averaged over our detection geometry by Monte Carlo calculation. The solid curve shows the EED* calculation for the coplanar point geometry. The counters at $\alpha_\gamma = 320°$ and 360° are 56° and 59° below the horizontal plane.

B. Photon energy spectra

The measured differential cross section versus photon energy for several photon counters at $T_\pi = 269$ MeV is shown in Fig. 6 and at $T_\pi = 324$ MeV in Fig. 7. In all cases, the spectra can be characterized as smoothly decreasing with increasing photon energy up to the highest photon energy, which is approximately 150 MeV. For convenience, we have indicated the E_γ (c.m.) energy scale along the top in each picture. There is no evidence of structure revealing the direct excitation of the $\Delta(1232)$ resonance. These features were also observed at $T_\pi = 298$ MeV, already discussed in I and II. The fact that the results at all three incident pion momenta have the same features removes any lingering notion there might be about a hypothetical accidental cancellation to explain our original data at $T_\pi = 298$ MeV. Various model calculations, indicated in Figs. 6 and 7, will be discussed in Sec. VI.

C. Differences between π^+ and π^- bremsstrahlung

To make the comparison between experiment and theory as nearly independent of experimental and theoretical uncertainties as possible, we have considered several ratios of experimental cross sections. The first of these is the π^--to-π^+ ratio at each kinematic point. We define the ratios

$$P_1 = \frac{d^5\sigma(\pi^-p\gamma \text{ at } 263 \text{ MeV})}{d^5\sigma(\pi^+p\gamma \text{ at } 269 \text{ MeV})}, \tag{3a}$$

$$P_2 = \frac{d^5\sigma(\pi^-p\gamma \text{ at } 298 \text{ MeV})}{d^5\sigma(\pi^+p\gamma \text{ at } 298 \text{ MeV})}, \tag{3b}$$

$$P_3 = \frac{d^5\sigma(\pi^-p\gamma \text{ at } 330 \text{ MeV})}{d^5\sigma(\pi^+p\gamma \text{ at } 324 \text{ MeV})}. \tag{3c}$$

Our measured value of P_1 for the photon energy interval $15 < E_\gamma < 30$ MeV versus the horizontal photon angle α_γ is shown in Fig. 8. We see that P_1 depends strongly on the position of the photon counter. A similar result characterizes P_1 obtained at other photon energies and also P_2 and P_3. It is interesting to compare P_1 with the ratio of the elastic differential cross sections at $T_\pi = 269$ MeV and $\theta_{\text{lab}}(\pi) = 52°$ obtained from Table V

$$\frac{d\sigma/d\Omega(\pi^-p\to\pi^-p)}{d\sigma/d\Omega(\pi^+p\to\pi^+p)} = 0.14.$$

Note that in the region of the dip in the $\pi^+p\gamma$ cross section near $\alpha_\gamma = 220°$ described in Sec. VA, the ratio P_1 is greater than unity.

The theoretical calculation of the ratio P and of other quantities of interest can be freed from dependence on the πp phase-shift solutions by normalizing the EED calculation to the values of the π^+ and π^- elastic cross sections measured in this experiment. Such normalized calculations are denoted EED*. The dashed line in Fig. 8 is the EED* calculation of P_1 for the coplanar point geometry. The Monte Carlo–averaged EED* predictions of counters that have the same α_γ are shown in the figure by solid circles.

Measured values of P for the three sets of incident pion energies, but now as a function of the photon energy, are shown in Figs. 9–11. The results for neighboring counters have been combined to improve statistics. The solid lines in these figures are again the EED* predictions and the dashed lines EED$(\overline{s},\overline{t})$ as defined in Sec. VI.

D. Dependence on incident pion energy

The ratios of our experimental cross sections in the laboratory system for the two new incident pion

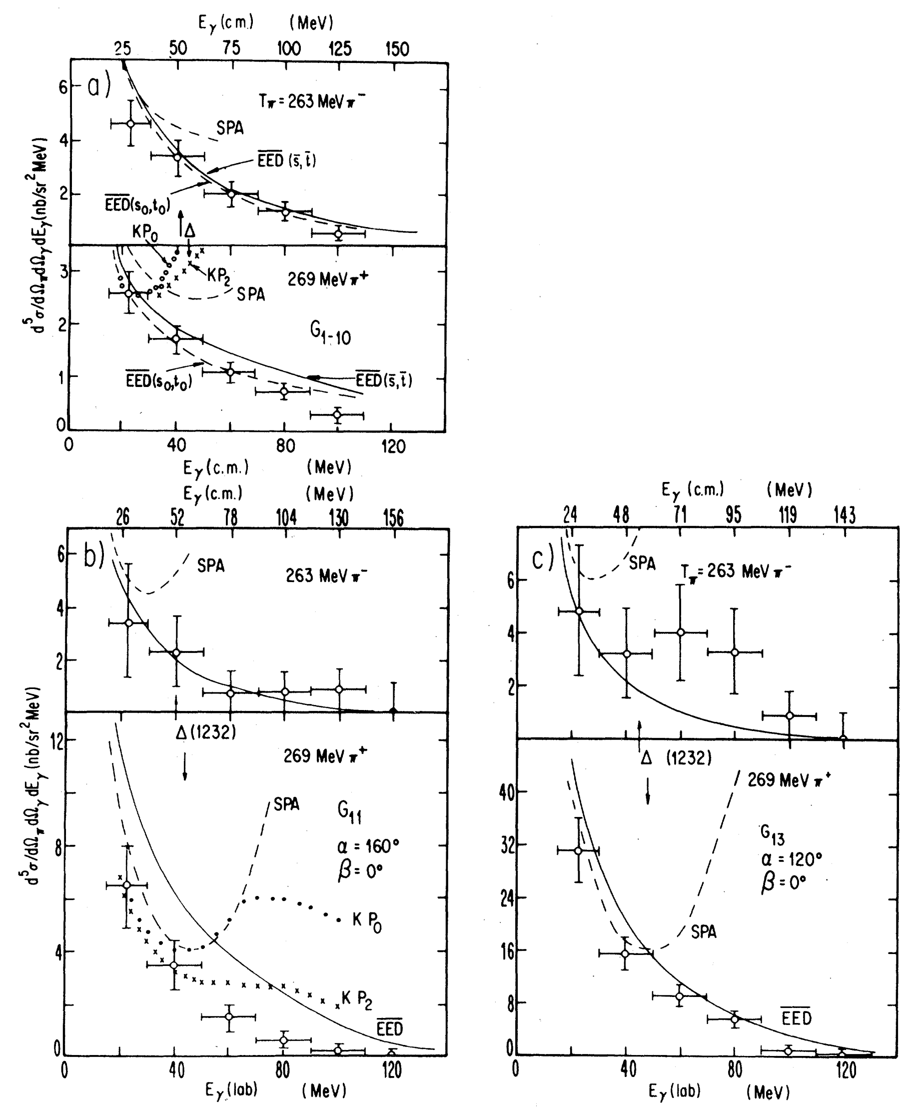

FIG. 6. Laboratory differential cross section versus photon energy for $\pi^+p\gamma$ and $\pi^-p\gamma$ at T_π = 269 and 263 MeV, respectively, for various photon counters. The theoretical curves are described in Sec. VI. EED = external-emission dominance (Ref. 20). SPA = soft-photon approximation as given in Ref. 4. $KP_{0,2}$ = Kondratyuk and Ponomarev (Ref. 12) model with $\mu_{\Delta^{++}} = 0, 2\mu_p$ respectively. The arrows marked Δ(1232) show the photon energy for which the final πp system has an invariant mass of 1232 MeV.

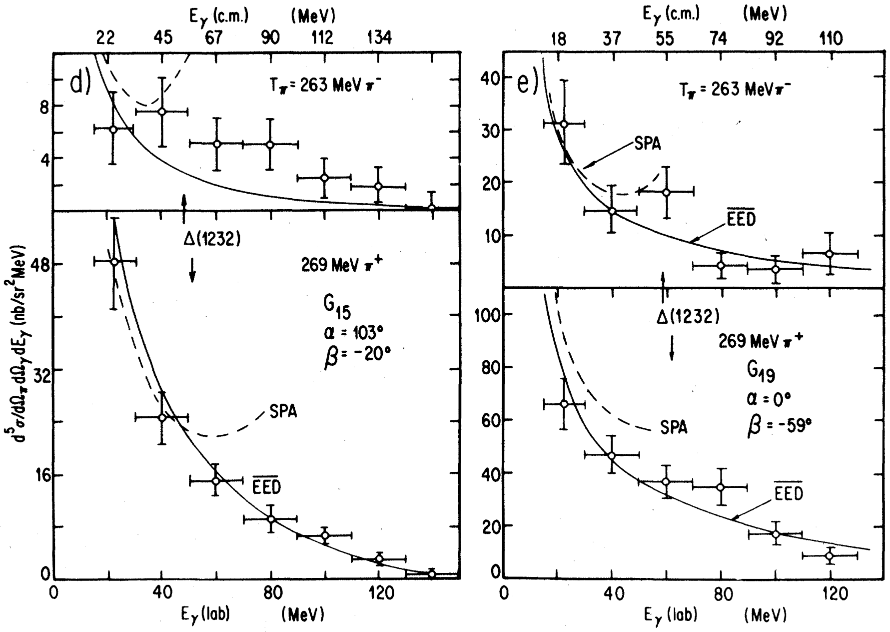

Fig. 6. (*Continued*)

energies are

$$R_+ = \frac{d^5\sigma(\pi^+p\gamma \text{ at } 269 \text{ MeV})}{d^5\sigma(\pi^+p\gamma \text{ at } 324 \text{ MeV})}, \tag{4a}$$

$$R_- = \frac{d^5\sigma(\pi^-p\gamma \text{ at } 263 \text{ MeV})}{d^5\sigma(\pi^-p\gamma \text{ at } 330 \text{ MeV})}. \tag{4b}$$

Figures 12 and 13 show these ratios as a function of photon energy in the lab. Note that the numerator and denominator are evaluated for the same photon energy interval in the lab but for different photon energies in the center of mass, so that this ratio is not a very fundamental quantity. The usefulness of R lies in the fact that it is free of several systematic experimental uncertainties. Like the ratio P, R_+ and R_- are best compared with calculations using the EED* procedure, and, like P, they show little variation with photon energy at any of the angles investigated. They provide added evidence that there is little of the expected contribution from the Δ(1232) resonance.

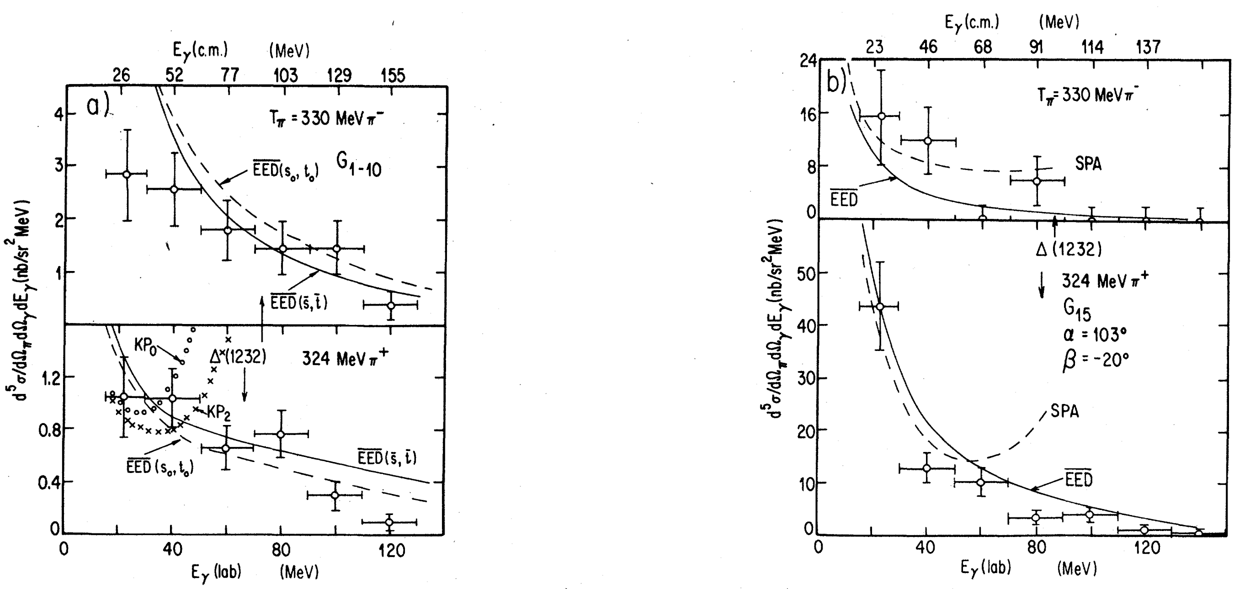

FIG. 7. Same as Fig. 6, except at T_{π^+} = 324 MeV and T_{π^-} = 330 MeV.

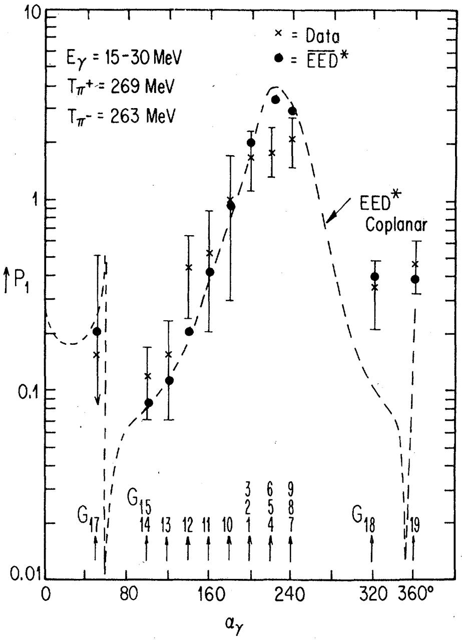

FIG. 8. Ratio P_1 of measured differential cross sections for the photon energy interval $E_\gamma = 15-30$ MeV, averaged over photon counters with the same α_γ, as a function of α_γ, the horizontally projected angle of the photon counters; $P_1 = d^5\sigma(\pi^- p\gamma$ at 263 MeV$)/d^5\sigma(\pi^+ p\gamma$ at 269 MeV$)$. The dashed curve is the EED* calculation for a coplanar geometry (see text). The dots are the $\overline{\text{EED}}$* calculation, averaged over the acceptance of our detectors. The vertical arrows on the abscissa indicate the position of the photon counters.

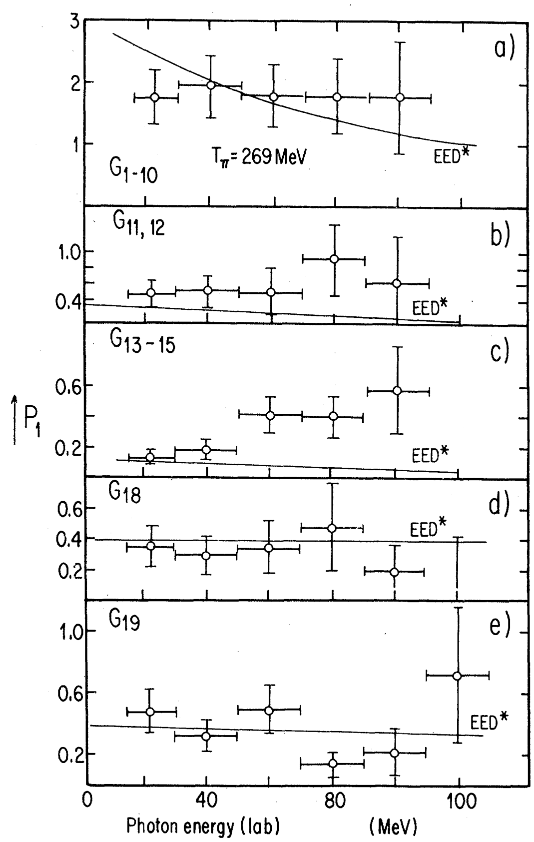

FIG. 9. Ratio P_1 of measured differential cross sections averaged over neighboring photon counters as a function of photon energy; $P_1 = d^5\sigma(\pi^- p\gamma$ at 263 MeV$)/d^5\sigma(\pi^+ p\gamma$ at 269 MeV$)$. The solid line is the EED* calculation for a point geometry.

E. The effect of detector size

Accurate comparison of our experimental results with a theoretical model necessitates taking into account the finite size of the detectors. The large horizontal and vertical acceptance of the pion spectrometer makes the consideration of detector size important. Among the consequences, we note that (a) the angle of the scattered pion with respect to the beam direction has a range of 44° to 59°, with an average value of 52° (as compared with the "coplanar central ray" angle of 50.5°) as a result of the large vertical acceptance of the spectrometer, and (b) even for the "coplanar" photon counters (G_1, G_4, G_7, G_{11}, G_{12}, G_{13}, and G_{14}), the acceptance includes many events rather far from coplanarity, and is not even coplanar *on the average* because the vertical bend of the spectrometer magnet introduces a vertical asymmetry in its acceptance.

In view of these large variations, the only reliable procedure for comparing the experimental results with theory is to average the theoretical predictions over the acceptance of the detectors by the Monte Carlo method. This procedure has been followed in most of the comparisons with the SPA and EED calculations discussed below.

In some cases, however, calculations are performed only in "point" geometry, i.e., with the scattered pion at 50.5° to the beam direction in the horizontal plane and the photon direction given by the position of the center of the counter as listed in Table I. This procedure is simpler and cheaper than the Monte Carlo treatment and is perhaps the only feasible method when the calculations are performed by theoretical physicists unfamiliar with the details of the apparatus.

To permit an easy estimation of the effects of the detector size on the measured cross sections, we have calculated the ratio of the Monte Carlo-averaged cross section to the point cross section using the EED calculation described in Sec. VI. The calculation is based on 1000 Monte Carlo-generated events, of which less than $\frac{1}{3}$ are accepted. The ratio

$$S = \frac{d^5\sigma(\pi p\gamma, \text{EED, Monte Carlo average})}{d^5\sigma(\pi p\gamma, \text{EED, point calculation})}$$

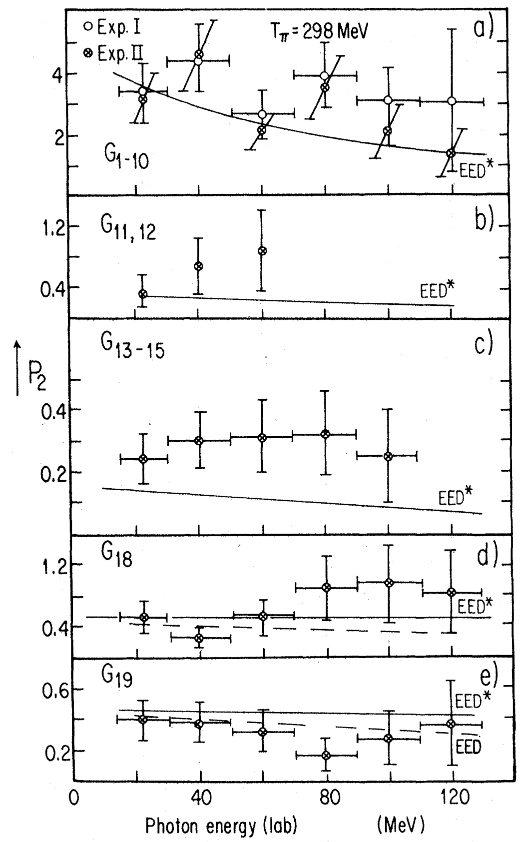

FIG. 10. Same as Fig. 9, except that $P_2 = d^5\sigma(\pi^- p\gamma$ at 298 MeV$)/d^5\sigma(\pi^+ p\gamma$ at 298 MeV). The two sets of data for the photon counters G_{1-10} in (a) are the revised results of Exps. I and II. The dashed lines in (d) and (e) are EED$(\bar{s}, \bar{t})$.

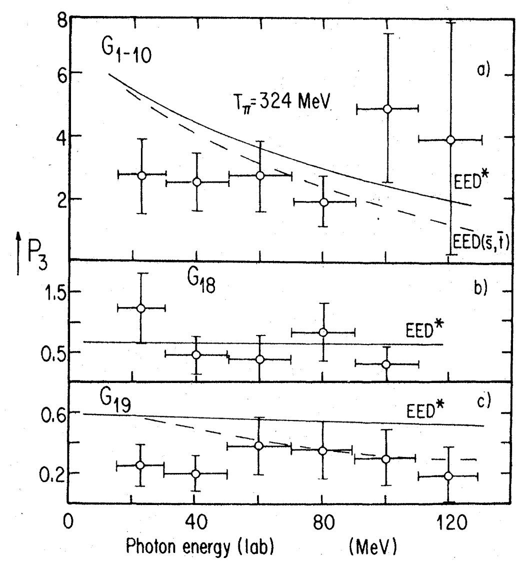

FIG. 11. Same as Fig. 9, except that $P_3 = d^5\sigma(\pi^- p\gamma$ at 330 MeV$)/d^5\sigma(\pi^+ p\gamma$ at 324 MeV).

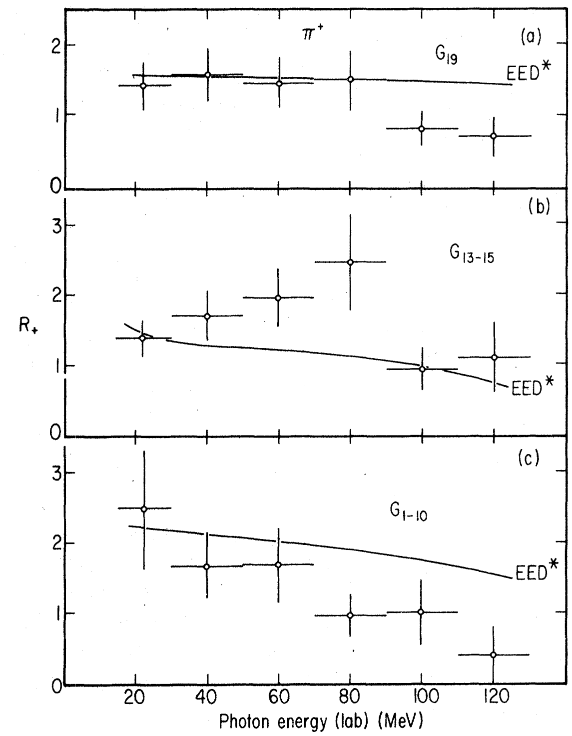

FIG. 12. Ratio R_+ versus photon energy for groups of neighboring photon counters. The solid curve is the EED* calculation. $R_+ = d^5\sigma(\pi^+ p\gamma$ at 269 MeV$)/d^5\sigma(\pi^+ p\gamma$ at 324 MeV).

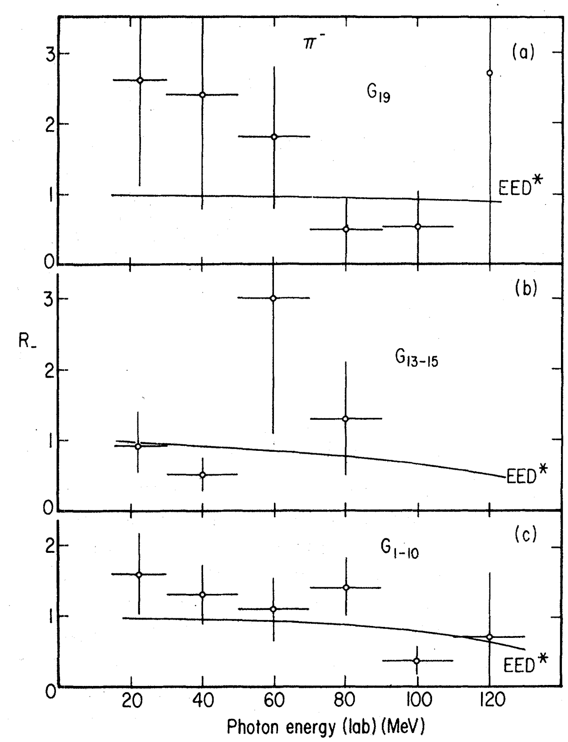

FIG. 13. Same as Fig. 12 except $R_- = d^5\sigma(\pi^- p\gamma$ at 263 MeV$)/d^5\sigma(\pi^- p\gamma$ at 330 MeV).

TABLE VI. Modification of coplanar point cross sections to take into account the finite aperture of our detectors. Listed are the calculated values of the ratio S for different photon counters at T_π = 324 MeV.

$$S=\frac{d^5\sigma(\pi p\gamma,\text{ EED, Monte Carlo average calculation})}{d^5\sigma(\pi p\gamma,\text{ EED, point calculation})}$$

Photon counter \ E_γ (MeV)	17.5		55		85		105		125	
	π^+	π^-	π^+	π^-	π^+	π^-	π^+	π^-	π^+	π^-
G_1	1.0	1.0	1.0	1.0	1.0	1.0	0.8	0.9	0.5	0.6
G_3	1.1	1.0	1.0	1.0	1.0	1.0	0.9	1.0	0.6	0.8
G_5	1.1	1.0	1.0	1.0	1.0	1.0	0.9	1.0	0.8	0.9
G_9	1.1	1.0	1.1	1.0	1.0	1.0	1.0	1.0	1.0	1.0
G_{10}	1.0	1.0	0.9	1.0	0.9	1.1	0.8	1.0	0.6	0.7
G_{11}	0.9	1.0	0.9	1.0	0.9	1.0	0.7	0.8	0.4	0.5
G_{13}	0.9	1.0	0.9	1.1	0.9	1.2	0.8	1.1	0.6	1.0
G_{17}	1.3	1.3	1.2	1.2	1.0	1.0	1.0	1.1	1.0	1.1
G_{18}	0.9	1.0	1.0	1.0	1.0	1.0	1.0	1.0	1.0	1.0

for $\pi^\pm p\gamma$ at 324 MeV is shown in Table VI. The accuracy of the first four columns is 5%; it gradually deteriorates to about 25% in the last column. The ratio deviates substantially from unity only at the high-E_γ end of the photon spectrum, where the acceptance is changing rapidly (Fig. 2), and the results are least reliable.

VI. COMPARISON WITH THEORETICAL CALCULATIONS

A. External-emission dominance

External-emission dominance (EED)[20] is a calculation in which the bremsstrahlung cross section is approximated by the first term of the Low expansion, and depends in a straightforward way on the elastic scattering cross section. In the center-of-mass system

$$\frac{d^5\sigma}{d\Omega_\pi d\Omega_\gamma dE_\gamma}=\frac{e^2}{2(2\pi)^3}\frac{\sqrt{s}}{|\vec{P}_1|}\frac{|\vec{P}_3|\,|\vec{K}|}{|\vec{P}_3|^2\sqrt{s}-|\vec{K}|)+E_3(\vec{P}_3\cdot\vec{K})}$$

$$\times A^\mu A_\mu \frac{d\sigma}{d\Omega}(s,t) \tag{5a}$$

with

$$A^\mu=\mp\frac{P_1^\mu}{P_1\cdot K}-\frac{P_2^\mu}{P_2\cdot K}\pm\frac{P_3^\mu}{P_3\cdot K}+\frac{P_4^\mu}{P_4\cdot K}\,, \tag{5b}$$

where P_1 and P_3 are the four-momenta of the incident and outgoing pion, P_2 and P_4 are the four-momenta of the proton, and K is the four-momentum of the photon. e^2 here is $4\pi/137$. The elastic cross section $d\sigma/d\Omega$ is evaluated at suitable values (see below) of s and t, where s = square of the total πp center-of-mass energy, and t = square of four-momentum transfer.

Among the virtues of EED are gauge and Lorentz invariance, the absence of adjustable parameters, and its computational simplicity. There is an ambiguity in the choice of s and t at which to evaluate the elastic cross section in Eq. (5a). One possibility, used frequently in soft-photon calculations (cf. Ref. 13), is to use the average values $\bar{s}$ and $\bar{t}$, where

$$\bar{s}=\tfrac{1}{2}[(P_1+P_2)^2+(P_3+P_4)^2]\,, \tag{6a}$$

$$\bar{t}=\tfrac{1}{2}[(P_1-P_3)^2+(P_2-P_4)^2]\,. \tag{6b}$$

In this paper the label EED implies the $(\bar{s},\bar{t})$ version of the calculation. Only where needed for emphasis have we written explicitly EED$(\bar{s},\bar{t})$. Another possibility is EED(s_0,t_0), where the fixed parameters s_0 and t_0 are chosen at the zero-photon-energy or elastic-scattering limit

$$s_0=(P_1+P_2)^2\,, \tag{7a}$$

$$t_0=(P_1-P_0)^2\,, \tag{7b}$$

with P_0 the four-momentum of a pion elastically scattered at 50.5°.

As discussed in the previous section, it is desirable to compare the data to the EED calculation averaged over the aperture of our detectors, for which we have used a Monte Carlo routine. Such calculations are labeled $\overline{\text{EED}}$ here.

For the numerical value of the elastic scattering cross section, we use a polynomial fit to the phase-shift calculations of Carter *et al.*,[26] supplemented by the Saclay phase-shift solutions[24] at energies above 292 MeV. There are sometimes perceptible differences between the EED$(\bar{s},\bar{t})$ and EED(s_0,t_0) calculation, as may be seen in Figs. 6(a) and 7(a), but all the important qualitative features of the EED calculation are insensitive to the choice of s and t.

Since the EED(s_0,t_0) calculation requires only one value of the elastic cross section for each incident energy, it is easy to normalize the EED(s_0,t_0) calculation to the elastic cross sections as measured in our own experiment (Sec. IV C). The resulting calculation is labeled EED*. This procedure has two advantages: (i) it eliminates any experimental normalization errors which are common to both the elastic and radiative measurement, and (ii) it removes the dependence of the calculation of the elastic πp phase-shift solutions. The latter point is important, because the most recent experimental data on πp elastic scattering in this energy region go only up to 292 MeV, so that calculations for our 298- and 324-MeV measurements require interpolation between phase-shift solutions based on several older experiments whose consistency is in doubt.

Our results are compared with EED calculations in Figs. 3 and 5–13. In general, the agreement is good up to the highest photon energy of 150 MeV, including in the region of destructive interference around $\alpha_\gamma \sim 220°$. EED accounts particularly well for the smoothly decreasing photon spectrum of Figs. 3, 6, and 7 and the rapidly changing photon angular distribution of Fig. 5. Less satisfactory, though still acceptable, is the agreement with the P and R ratios, especially for photon counters G_{13-15} (Figs. 9–13).

B. Soft-photon approximation

In contrast to EED, in which only the first term of order $1/E_\gamma$ is evaluated, the soft-photon approximation (SPA) consists of the first *two* terms of the Low expansion[11] of the bremsstrahlung amplitude [Eq. (1)]. The treatment of the second term is open to many uncertainties at high photon energy. The recipe used by us in I (see Ref. 4) calls for the separate evaluation of the photon emission by the proton and the pion. The delicate cancellation of the pion and proton bremsstrahlung amplitudes, which causes the big dip in the differential cross section around $\alpha_\gamma = 220°$ as $E_\gamma \to 0$ (compare Fig. 4), does not occur in this formulation when the photon energy is >40 MeV for 269-MeV incident pions. As a result, the SPA prediction of Ref. 4, which is compared to our data in Figs. 6 and 7, shows a rise in the differential cross section which is not seen in our data. SPA works very well for our lowest photon energy interval $15 < E_\gamma < 30$ MeV, but it fails badly above $E_\gamma \sim 40$ MeV.

Recently, Liou and Nutt[27] have proposed a modified SPA recipe. They expand the bremsstrahlung amplitude, phase-space factor, proton projection operator, etc., in a form that is independent of E_γ in first order. The algebra involved is rather lengthy and thus far the calculations have been made only for coplanar geometry. Shown in Fig. 14 is the $\pi^+ p\gamma$ differential cross section at $T_\pi = 324$ for photon counters G_1 and G_{13} together with the

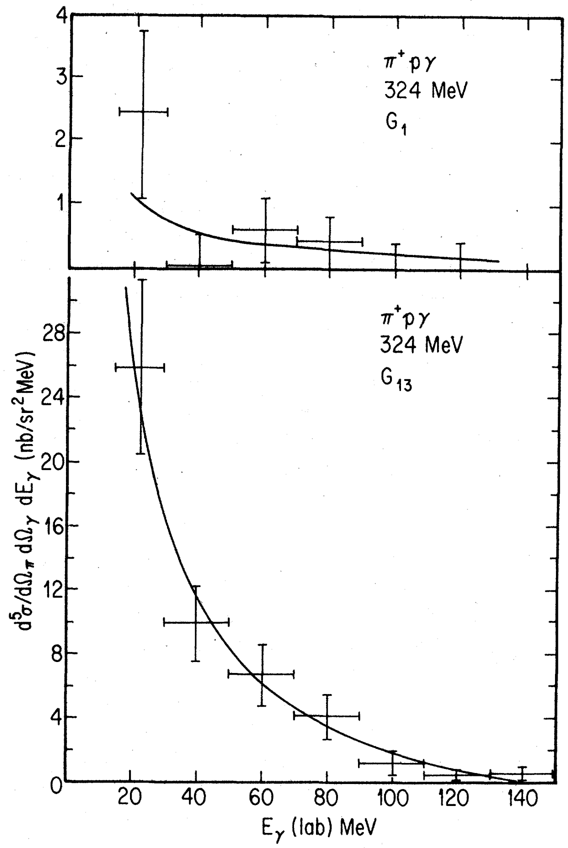

FIG. 14. $\pi^+ p\gamma$ laboratory differential cross sections versus photon energy at $T_\pi = 324$ MeV for photon counters G_1 and G_4. The solid line is the SPA calculation by Liou and Nutt. (Ref. 27).

SPA calculation of Liou and Nutt. The agreement is very good.

C. Magnetic dipole moment of the $\Delta^{++}(1232)$ resonance

One of the most interesting aspects of studying $\pi^+ p\gamma$ is undoubtedly the investigation of the magnetic dipole moment $\mu_{\Delta^{++}}$ of the $\Delta^{++}(1232)$ resonance, a quantity which cannot be measured by the conventional spin precession or atomic x-ray methods because of the short lifetime of the Δ. Beg, Lee, and Pais[19] have shown that SU(6) symmetry, which correctly predicts the ratio of the neutron and proton magnetic dipole moments, implies the relation

$$\mu_{10} = q\mu_p .$$

μ_{10} is the magnetic dipole moment of a member of the baryon spin-$\frac{3}{2}$ decuplet having an electric charge q, μ_p is the magnetic dipole moment of the proton, $\mu_p = 2.79\mu_N$, and $\mu_N = e\hbar/2m_p c$. Thus, the SU(6) prediction is $\mu_{\Delta^{++}} = 5.58\mu_N$. [The effect of the SU(6) breaking has been considered by Beg and Pais.[28] Applying their suggested correction for the baryon octet to the decuplet, we may obtain a modified SU(6) prediction $(\mu_{\Delta^{++}})_m = (m_p/m_\Delta)\, 5.58\mu_N = 4.25\mu_N$.]

The first explicit calculation relating $\mu_{\Delta^{++}}$ to a measurement of $\pi^+p\gamma$ was made by Kondratyuk and Ponomarev [12](KP) in 1968. They proposed measuring the differential cross section at 300-MeV incident π^+ energy with photons emerging near $\alpha_\gamma \simeq 220°$, the region of the minimum in the external bremsstrahlung contribution to the cross section (Sec. V A). This consideration played an important role in the design of our experiment. Figure 15 shows the Feynman diagram of the process that is crucial in the KP calculation. It is the radiative decay of the Δ to itself, which is allowed because of the large mass width of the Δ

$$\Delta^{++} \rightarrow \Delta^{++} + \gamma\,,$$

and as a consequence the $\pi^+p\gamma$ is a strong function of $\mu_{\Delta^{++}}$. Unfortunately, the KP prediction differs vastly from our measurements, not only from the results of Exp. I but equally dramatically from the new data. Figures 6(a), 6(b), and 7(a) show the KP prediction, including the correction by Vanzha *et al.*[12] for $\mu_{\Delta^{++}} = 0$ and $2\mu_p$. For either value of $\mu_{\Delta^{++}}$, KP predict a large bump in the photon spectrum for photon counters $G_{1\text{-}10}$ that goes far outside the scale of Figs. 6(a) and 7(a). Clearly, such a bump is not present in the data.

Using a modified Low theorem, Fischer and Minkowski[13] (FM) also predict a large Δ-resonance bump in the photon spectrum for $G_{1\text{-}10}$ which goes outside the scale of Figs. 6(a) and 7(a). Their prediction has been presented in I and is not shown here.

In a recent preprint, Pascual and Tarrach[18] (PT) have proposed a simple and elegant calculation which leads to surprisingly narrow limits for $\mu_{\Delta^{++}}$. PT argue that the absence of a bump or interference pattern in all our $\pi p\gamma$ photon spectra implies that the radiative decay $\Delta^{++} \rightarrow \Delta^{++}\gamma$ does not dominate the bremsstrahlung reaction. Imposing gauge invariance in the manner of KP and FM introduces

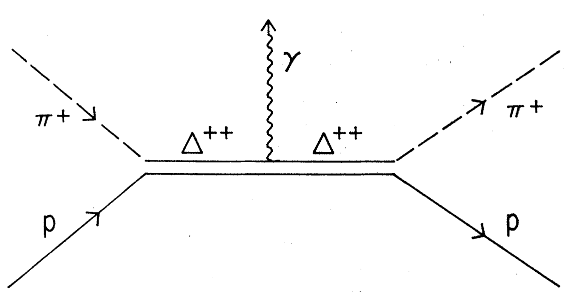

FIG. 15. Feynman diagram for the process $\pi^+p \rightarrow \Delta^{++} \rightarrow \Delta^{++}\gamma \rightarrow \pi^+p\gamma$.

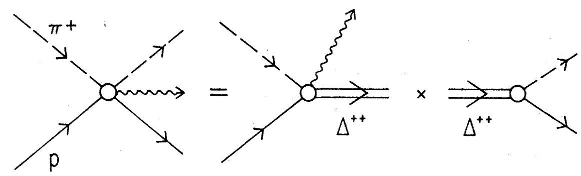

FIG. 16. Feynman diagram of the dominant contribution to $\pi^+p\gamma$ according to Pascual and Tarrach (Ref. 18). The amplitude is given by the product of the $\pi^+p \rightarrow \Delta^{++}\gamma$ amplitude for an on-mass shell Δ^{++} times the $\Delta^{++} \rightarrow p\pi^+$ vertex.

ambiguities that are unavoidable and nonnegligible. PT propose to calculate the $\mu_{\Delta^{++}}$ contribution to *$\pi^+p\gamma$ at one photon energy only, specifically, such that the π^+p final state is at the peak of the Δ^{++}(1232).* For this special photon energy, the dominant contribution to the $\pi^+p\gamma$ amplitude can be written as the product of the amplitude for the reaction $\pi^+p \rightarrow \Delta^{++}\gamma$ multiplied by the vertex for $\Delta^{++} \rightarrow \pi^+p$ (see Fig. 16) and a propagator that takes into account the finite width of the Δ. The process $\pi^+p \rightarrow \Delta^{++}\gamma$ can be calculated exactly in the first two orders in the photon energy expansion by using the Low theorem. This calculation depends only on the electric charges and magnetic dipole moments of p, π^+, and Δ^{++} of which only $\mu_{\Delta^{++}}$ is unknown. The $\mu_{\Delta^{++}}$-dependent contribution to $\pi^+p\gamma$ when the photon energy is such that the final-state π^+p is at the peak of the Δ can be expressed as

$$d^5\sigma/d\Omega_\pi d\Omega_\gamma dE_\gamma = a + b\mu_{\Delta^{++}} + c\mu_{\Delta^{++}}^2\,. \qquad (8)$$

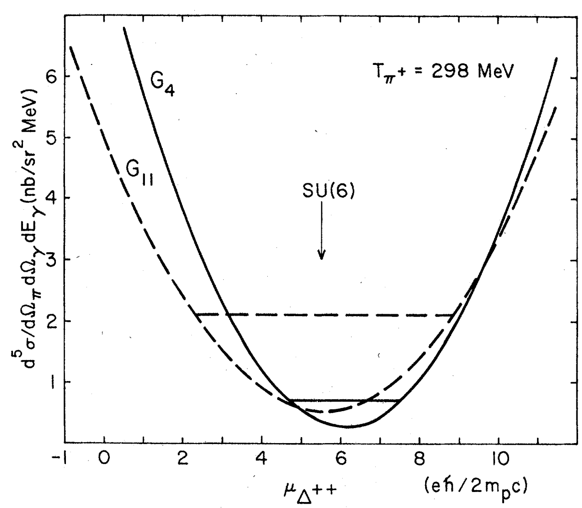

FIG. 17. $\pi^+p \rightarrow \pi^+p\gamma$ laboratory differential cross section for photon counters G_4 and G_{11} at $T_{\pi^+} = 298$ MeV for the photon energy at the resonance, $E_\gamma = 60$ and 58 MeV for G_4 and G_{11}, respectively, as a function of the magnetic dipole moment $\mu_{\Delta^{++}}$ of the $\Delta(1232)$ resonance calculated by Pascual and Tarrach (Ref. 18). The horizontal lines indicate our measured cross section including the quoted error (Exp. I). The vertical arrow indicates the SU(6) prediction.

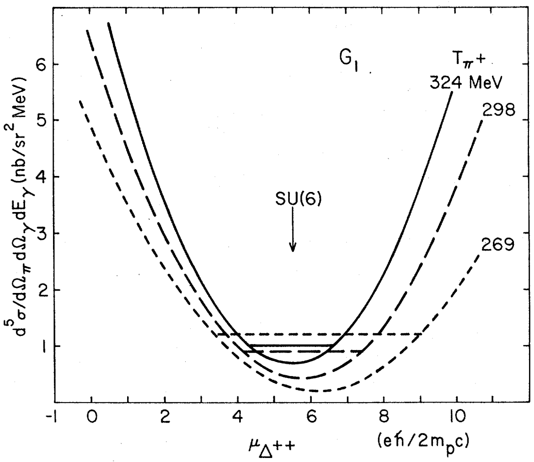

FIG. 18. Same as Fig. 17 except that the photon counter is G_1, $T_{\pi^+}=269$, 298, and 324 MeV, and the respective photon energy 43, 58, and 69 MeV.

The coefficients a, b, and c are easily calculated and are given in Ref. 19 for some of our coplanar counters. The $\pi^+p\gamma$ differential cross section calculated using Eq. (8) for photon counters G_4 and G_{11} at $T_\pi = 298$ MeV for the photon energy at the resonance, $E_\gamma = 60$ and 58 MeV for G_4 and G_{11}, respectively, versus $\mu_{\Delta^{++}}$ is shown in Fig. 17. There is a deep minimum in the cross section when $\mu_{\Delta^{++}} \simeq 6\ \mu_N$ and its smallness "explains" the absence of a bump or interference in our photon spectra, see Figs. 3, 6, and 7. Three more cases of the use of Eq. (8) are shown in Fig. 18, which is similar to Fig. 17 except that $T_\pi = 269$, 298, and 324 MeV, the photon counter is G_1 and the photon energy is 43, 58, and 69 MeV, respectively.

If one assumes that various possible $\pi^+p\gamma$ diagrams, not considered by PT in calculating Eq. (8), are unimportant, one can use our measured differential cross section to place limits on the magnitude of $\mu_{\Delta^{++}}$ as shown in Figs. 17 and 18. The cross sections measured in our experiment, including the quoted errors, are indicated in both figures by the horizontal lines. Their intersections with the respective curves provide reasonable limits for $\mu_{\Delta^{++}}$. The results are listed in Table VII. The tightest limits are

$$+4.7 < \mu_{\Delta^{++}} < 6.7\ \mu_N ; \tag{9}$$

they are obtained by combining the values for the photon counters G_1 and G_4, located near $\alpha_\gamma \simeq 220°$ where external emission is the smallest.

The limits obtained for all our coplanar counters (the only ones calculated by PT) at all three incident pion energies, are consistent with Eq. (9), which enhances our confidence in the PT model. The magnitude and sign of $\mu_{\Delta^{++}}$ given in Eq. (9) are in excellent agreement with the SU(6) prediction of $+5.6\ \mu_N$.

Among the shortcomings of the PT calculation is the incomplete treatment of the effects of the short lifetime of the Δ and the neglect of the radiation of the outgoing π and p in the calculation. In view of the steepness of the curves in Figs. 17 and 18, we do not believe that the inclusion of the neglected terms will cause a substantial change in the above-quoted limits for $\mu_{\Delta^{++}}$. Crucial to the PT calculation is the applicability of the Low-type expansion in the photon energy when the photon energy can be as high as 78 MeV. It has been shown recently[29] that SPA based on the Low expansion is

TABLE VII. Limits for the magnetic dipole moment of the Δ^{++} (1232) resonance obtained using the model of Pascual and Tarrach (Ref. 18). The fourth column gives our experimental results of $d^5\sigma/d\Omega_\pi d\Omega_\gamma dE_\gamma$ increased by the quoted error, obtained at the photon energy corresponding to the peak of the Δ^{++} which is given in column 3.

Photon counter G	Incident π^+ energy (MeV)	Photon energy lab (MeV)	$d^5\sigma/d\Omega_\pi d\Omega_\gamma dE_\gamma(\pi^+p\gamma)$ our exp. (nb/sr^2 MeV)	Limits on $\mu_{\Delta^{++}}$ $(e\hbar/2m_pc)$
1	269	44	1.2	$+3.3 < \mu_{\Delta^{++}} < 9.0$
4	269	45	1.6	$+3.6 < \mu_{\Delta^{++}} < 9.7$
1	298	58	0.9	$+4.2 < \mu_{\Delta^{++}} < 7.2$
4	298	60	0.7	$+4.7 < \mu_{\Delta^{++}} < 7.2$
11	298	58	2.1	$+2.4 < \mu_{\Delta^{++}} < 8.8$
12	298	60	3.9	$+0.8 < \mu_{\Delta^{++}} < 10$
1	324	69	1.0	$+4.2 < \mu_{\Delta^{++}} < 6.7$
4	324	72	1.4	$+4.1 < \mu_{\Delta^{++}} < 7.7$
7	324	78	1.6	$+4.6 < \mu_{\Delta^{++}} < 7.9$
11	324	69	1.1	$+4.1 < \mu_{\Delta^{++}} < 6.8$
12	324	72	2.5	$+2.4 < \mu_{\Delta^{++}} < 8.7$
13	324	78	6	$+0.3 < \mu_{\Delta^{++}} < 11$

applicable for photon energies in excess of 80 MeV in $pp \to pp\gamma$ at 730 MeV, and the present work shows that EED based on the first term of a Low-type expansion works still in $\pi^\pm p\gamma$ when $E_\gamma \sim 150$ MeV, implying that the Low expansion in the photon energy region used by PT is applicable.

It would be of interest to expand the PT model to $\pi^- p\gamma$ in the region of the $\Delta^0(1232)$ and investigate the sensitivity to μ_{Δ^0}. The magnitude of μ_{Δ^0} is predicted to be zero by SU(6).

A very interesting isobar model calculation of $\pi^+ p\gamma$ was made a few years ago by Musakhanov.[30] He made use of PCAC and current algebra to study the soft-pion limit of the $\pi p\gamma$ amplitude and related a number of parameters in this amplitude to the amplitude for neutrino-induced pion production. He found that there is a large cancellation in the contribution of the $\mu_{\Delta^{++}}$-dependent term to the cross section when $\mu_{\Delta^{++}} \simeq 6\ \mu_N$. Musakhanov's analysis of our preliminary results reported in Ref. 1 yields the value $\mu_{\Delta^{++}} = (3.6 \pm 2)\ \mu_N$ consistent with the limits given in Eq. (9).

D. Model calculations

In addition to those calculations discussed in the preceding sections, $\pi p\gamma$ has over the years been the subject of a variety of model calculations which fall into two categories.

(a) Papers written before our first experimental results were available. The detailed calculations in this category all predict a resonance bump in the photon spectrum. Examples are the work of Cutkosky[31] and Carruthers[32] based on the static model, and the calculation of Baier *et al.*[33] based on an effective Lagrangian.

(b) Calculations performed after our results were published. They face the challenge of explaining the pertinent features of the data, namely, small differential cross sections that decrease smoothly with increasing photon energy.

Thompson[14] uses a nonrelativistic current operator in a simple static model calculation and argues that the $\Delta(1232)$ resonance, because of its broad width, does not manifiest itself as a bump in the photon spectrum of $\pi^+ p\gamma$.

Beder[15] has examined a large number of modifications to the basic Lagrangian recipe used extensively in the literature, including the important $\pi p\gamma$ calculations by Kondratyuk and Ponomarev.[12] He finds that various reasonable modifications of the basic Lagrangian do not remove the vast discrepancy between our data and theory.

Bosco *et al.*[16] use the Chew-Low model in a $\pi^+ p\gamma$ calculation in which the Δ does not manifest itself as a bump in the photon spectrum because of interference between various amplitudes and a large rescattering correction. They report agreement for photon counter G_4. However, there appear to be difficulties for G_{13}.

Ho-Kim and Lavine[17] also use the Chew-Low model, but their calculated photon spectra have a bump that is connected with the Δ resonance. A typical example is presented in Fig. 19. The predicted photon spectra in G_4 are shown for the three π^+ energies reported here. For comparison, we have included our Exp. I results, which have the smallest errors.

We can summarize the situation as follows: A satisfactory dynamical calculation of $\pi p\gamma$ that agrees with our data is not yet available.

E. Off-mass-shell matrix elements

The reaction $\pi^- p \to \pi^- p\gamma$ has been recommended[34] as being particularly suitable for studying the important off-shell effects in pion-nucleon scattering. The contribution to $\pi^- p$ bremsstrahlung from external graphs is nearly gauge invariant; the Δ^0 intermediate state is neutral and presumably does not radiate [the SU(6) prediction for its magnetic moment is 0], and, furthermore, the interference among the four contributions from the external lines is constructive so that the matrix element is not subject to the delicate cancellations which are prominent in $\pi^+ p \to \pi^+ p\gamma$. Picciotto[34] has considered the case where the initial proton is virtual and the off-shell electromagnetic vertex has the form proposed by Bincer.[35] He introduces two form factors that can be related using threshold

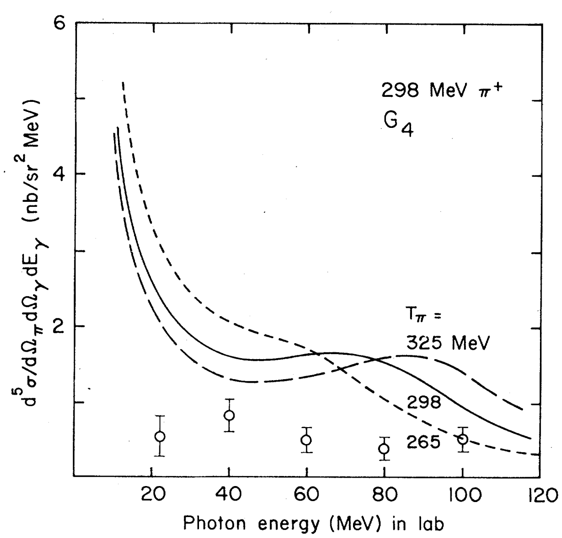

FIG. 19. $\pi^+ p\gamma$ laboratory differential-cross-section curves calculated by Ho-Kim and Lavine (Ref. 17) as a function of the photon energy for photon counter G_4 at $T_\pi = 265$, 298, and 325 MeV. The data points are our measurements at $T_{\pi^+} = 298$ MeV, Exp. I.

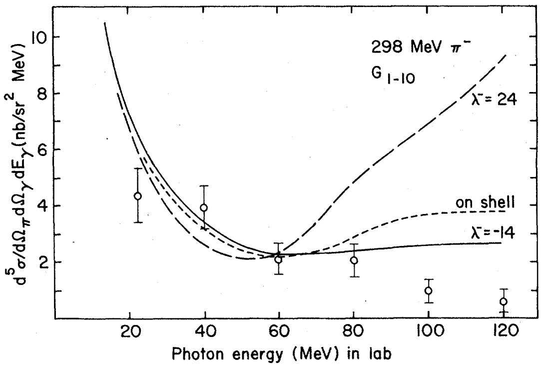

FIG. 20. $\pi^- p\gamma$ laboratory differential-cross-section curves calculated by Picciotto (Ref. 34) for G_{1-10} at $T_\pi = 298$ MeV versus photon energy for three values of the off-mass-shell parameter λ^-. The data points are our measurements at $T_\pi = 298$ MeV, Exp. I.

dominance, leaving only one unknown form factor λ^-. Picciotto's predictions, evaluated for three values of λ^- for counters G_{1-10} and 298-MeV incident π^-, are shown in Fig. 20 together with our data of Exp. I. Our data favor a negative value of λ^-, although exchange currents and off-shell effects in the πN amplitude, which were not considered by Picciotto, could affect this conclusion.

VII. CONCLUSIONS

Our measurements of $\pi^\pm p \to \pi^\pm p\gamma$ at $T_\pi = 269$, 298, and 324 MeV at 18 different photon angles show that the differential cross section decreases monotonically with increasing photon energy and that none of the spectra indicate any evidence for a final-state πp interaction involving the $\Delta(1232)$ resonance. The soft-photon approximation used in Ref. 4 is valid for photon energies up to about 40 MeV only. The soft-photon-approximation calculation proposed by Liou and Nutt is applicable for hard photons including the region of the strong $\Delta^{++}(1232)$ resonance, up to the highest photon energy of this experiment, $E_\gamma = 150$ MeV. The external-emission-dominance calculation gives an excellent account of all gross features of $\pi^\pm p$ bremsstrahlung: the dependence on sign and incident energy of the pion and on the angle and energy of the photon, up to the highest photon energy measured here. However, EED is sometimes imperfect in predicting the absolut cross sections.

Assuming the validity of the Pascual-Tarrach model, our measurements show that the magnetic dipole moment of the $\Delta^{++}(1232)$ resonance is $+4.7\mu_N < \mu_{\Delta^{++}} < +6.7\mu_N$, where $\mu_N = e\hbar/2m_p c$. Sign and magnitude are in agreement with the SU(6) prediction of $+5.6\mu_N$.

There is not yet available a satisfactory dynamical model to explain our $\pi^\pm p\gamma$ results, and the extraction of the off-mass-shell amplitudes awaits further theoretical work.

ACKNOWLEDGMENTS

We gratefully acknowledge the hospitality extended to us at the Lawrence Berkeley Laboratory and the assistance of the crew of the 184-in cyclotron. We thank Dr. D. Blasberg, Dr. B. Schrock, and Dr. J. Sperinde for their help in the intial phase of the experiment, J. Hartlove and S. Jarrett for help in data taking, M. O'Neill and the late M. Thimel for their contributions to the data analysis. Dr. P. Pascual has kindly provided us with the theoretical curves shown in Figs. 17 and 18 and Dr. M. K. Liou the curves shown in Fig. 14. This work was performed under the auspices of the U. S. Department of Energy.

---

*Present address: Department of Physics, Pahlavi University, Shiraz, Iran.
†Present address: Lawrence Berkeley Laboratory, Berkeley, California 94720.
‡Present address: Computer Sciences Corp., Silver Spring, Maryland 20910.
§Present address.

[1]M. Arman, D. J. Blasberg, R. P. Haddock, K. C. Leung, B. M. K. Nefkens, B. L. Schrock, D. I. Sober, and J. M. Sperinde, Phys. Rev. Lett. 29, 962 (1972).
[2]M. Arman, Ph.D. thesis, University of California, Los Angeles, 1972 (unpublished).
[3]B. M. K. Nefkens, M. Arman, P. Glodis, R. P. Haddock, K. C. Leung, B. L. Schrock, D. I. Sober, and J. W. Sperinde, in *High Energy Physics and Nuclear Structure, Proceedings of the Fifth International Conference, Uppsala, Sweden, 1973*, edited by G. Tibell (North-Holland, Amsterdam, 1974), p. 51.
[4]D. I. Sober, M. Arman, D. J. Blasberg, R. P. Haddock, K. C. Leung, B. M. K. Nefkens, B. L. Schrock, and J. M. Sperinde, Phys. Rev. D 11, 1017 (1975) (referred to as I).
[5]K. C. Leung, M. Arman, H. C. Ballagh, P. F. Glodis, R. P. Haddock, B. M. K. Nefkens, and D. I. Sober, Phys. Rev. D 14, 698 (1976) (referred to as II).
[6]J. Deahl *et al.*, Phys. Rev. 124, 1987 (1961).
[7]V. E. Barnes *et al.*, CERN Report No. 63-27, 1963 (unpublished).
[8]J. Debaisieux *et al.*, Nucl. Phys. 63, 273 (1965).
[9]R. T. Van de Walle *et al.*, Nuovo Cimento 53A, 745 (1968).
[10]T. D. Blokhintseva *et al.*, Yad. Fiz. 8, 928 (1968) [Sov. J. Nucl. Phys. 8, 539 (1969)].
[11]F. E. Low, Phys. Rev. 110, 974 (1958).
[12]L. A. Kondratyuk and L. A. Ponomarev, Yad. Fiz. 7, 111 (1968) [Sov. J. Nucl. Phys. 7, 82 (1968)]; modified by A. Vanzha and M. Musakhanov, Dubna Report No. JINR-R2-6306, 1972 (unpublished).

[13]W. E. Fischer and P. Minkowski, Nucl. Phys. B36, 519 (1972).
[14]R. H. Thompson, Nuovo Cimento 16A, 290 (1973).
[15]D. Beder, Nucl. Phys. B84, 362 (1975).
[16]B. Bosco, A. Conti, G. Landi, and F. Matera, Phys. Lett. 60B, 47 (1975).
[17]Q. Ho-Kim and J. P. Lavine, Phys. Lett. 60B, 269 (1976); Nucl. Phys. A285, 407 (1977).
[18]P. Pascual and R. Tarrach, Nucl. Phys. B134, 133 (1978).
[19]M. A. B. Beg, B. W. Lee, and A. Pais, Phys. Rev. Lett. 13, 514 (1964).
[20]B. M. K. Nefkens and D. I. Sober, Phys. Rev. D 14, 2434 (1976).
[21]W. H. Barkas and M. J. Berger, in Nuclear Science Series Report No. 39, National Acad. of Sciences–National Res. Council Publ. 1133, 1964 (unpublished), pp. 103–172.
[22]D. I. Sober, M. Arman, D. J. Blasberg, R. P. Haddock, K. C. Leung, and B. M. K. Nefkens, Nucl. Instrum. Methods 108, 573 (1973).
[23]P. J. Bussey, J. R. Carter, D. R. Dance, D. V. Bugg, and A. A. Carter, Nucl. Phys. B58, 378 (1973).
[24]Saclay solution (1974), from Particle Data Group phase-shift tape, LBL, Berkeley, 1974 (unpublished); R. Kelly, private communication.
[25]V. A. Gordeev *et al.*, in *Meson-Nuclear Physics—1976*, Proceedings of the International Topical Conference, Carnegie-Mellon Univ., edited by P. D. Barnes, R. A. Eisenstein, and L. S. Kisslinger (AIP, New York, 1976), p. 36.
[26]J. Carter, D. Bugg, and A. Carter, Nucl. Phys. B58, 378 (1973).
[27]M. K. Liou and W. T. Nutt, Phys. Rev. D 16, 2176 (1977).
[28]M. Beg and A. Pais, Phys. Rev. 137, B1516 (1965).
[29]B. M. K. Nefkens, in *Nucleon-Nucleon Interactions—1977*, proceedings of the Second International Conference, Vancouver, 1977, edited by H. Fearing, D. Measday and A. Strathdee (AIP, New York, 1978).
[30]M. M. Musakhanov, Yad. Fiz. 19, 630 (1974) [Sov. J. Nucl. Phys. 19, 319 (1974)].
[31]R. E. Cutkosky, Phys. Rev. 113, 727 (1959).
[32]P. Carruthers, Phys. Rev. 134, B638 (1964).
[33]R. Baier, L. Pittner, and P. Urban, Nucl. Phys. B27, 589 (1971).
[34]Ch. Picciotto, Nuove Cimento 29A, 41 (1975).
[35]A. M. Bincer, Phys. Rev. 112, 855 (1958).